Nucleosomes and DNA methylation shape meiotic DSB frequency in Arabidopsis transposons and gene regulatory regions

Kyuha Choi[1,†], Xiaohui Zhao[1], Christophe Lambing[1], Charles J. Underwood[1,2], Thomas J. Hardcastle[1], Heïdi Serra[1], Andrew J. Tock[1], Piotr A. Ziolkowski[1], Nataliya E. Yelina[1], Robert A. Martienssen[2] and Ian R. Henderson[1*]

[1] Department of Plant Sciences, University of Cambridge, Cambridge, Cambridgeshire, CB2 3EA, United Kingdom.

[2] Howard Hughes Medical Institute-Gordon and Betty Moore Foundation, Watson School of Biological Sciences, Cold Spring Harbor Laboratory, Cold Spring Harbor, New York, USA.

Corresponding Author

* Ian R. Henderson (irh25@cam.ac.uk)

† Current address: Department of Life Sciences, Pohang University of Science and Technology, Pohang, Gyeongbuk, 37673, Republic of Korea.

Keywords

Meiosis, recombination, DSB, hotspot, SPO11-1, crossover, nucleosomes, DNA methylation, H3K4^{me3}, transposons.

Abstract

Meiotic recombination initiates via DNA double strand breaks (DSBs) generated by SPO11 topoisomerase-like complexes. Recombination frequency varies extensively along eukaryotic chromosomes, with hotspots controlled by chromatin and DNA sequence. To map meiotic DSBs throughout a plant genome, we purified and sequenced Arabidopsis SPO11-1-oligonucleotides. DSB hotspots occurred in gene promoters, terminators and introns, driven by AT-sequence richness, which excludes nucleosomes and allows SPO11-1 access. A strong positive relationship was observed between SPO11-1 DSBs and final crossover levels. Euchromatic marks promote recombination in fungi and mammals, and consistently we observe H3K4^{me3} enrichment in proximity to DSB hotspots at gene 5'-ends. Repetitive transposons are thought to be recombination-silenced during meiosis, in order to prevent non-allelic interactions and genome instability. Unexpectedly, we found strong DSB hotspots in nucleosome-depleted Helitron/Pogo/Tc1/Mariner DNA transposons, whereas retrotransposons were coldspots. Hotspot transposons are enriched within gene regulatory regions and in proximity to immunity genes, suggesting a role as recombination-enhancers. As transposon mobility in plant genomes is restricted by DNA methylation, we used the *met1* DNA methyltransferase mutant to investigate the role of heterochromatin on the DSB landscape. Epigenetic activation of transposon meiotic DSBs occurred in *met1* mutants, coincident with reduced nucleosome occupancy, gain of transcription and H3K4^{me3}. Increased *met1* SPO11-1 DSBs occurred most strongly within centromeres and Gypsy and CACTA/EnSpm coldspot transposons. Together, our work reveals complex interactions between chromatin and meiotic DSBs within genes and transposons, with significance for the diversity and evolution of plant genomes.

Introduction

Sexual eukaryotes reproduce via fusion of haploid gametes, which are produced by the specialized meiotic cell division. During meiosis a single round of DNA replication is coupled to two rounds of chromosome segregation. Additionally, during prophase of the first meiotic division, homologous chromosomes pair and recombine, which can result in reciprocal crossovers (Kauppi et al. 2004; Villeneuve and Hillers 2001). As a consequence of recombination and independent chromosome segregation, meiosis has a major effect on genetic variation within populations and the process of evolutionary adaptation (Barton and Charlesworth 1998; Hamilton 2002).

Meiotic recombination initiates via formation of DNA double strand breaks (DSBs), which can be repaired using a homologous chromosome to produce crossover or non-crossover products (Kauppi et al. 2004; Baudat et al. 2013; Villeneuve and Hillers 2001; Szostak et al. 1983). Meiotic DSBs are universally generated by SPO11 topoisomerase-like transesterases, which act as dimers to cleave opposite phosphodiester backbones using catalytic tyrosine residues (Neale et al. 2005; Keeney and Kleckner 1995; Pan et al. 2011; Keeney et al. 1997). In plants, SPO11-1 and SPO11-2 interact with MEIOTIC TOPOISOMERASE VIB (MTOPVIB), which forms a conserved catalytic core complex (Robert et al. 2016; Vrielynck et al. 2016; Hartung et al. 2007; Grelon et al. 2001). Following phosphodiester cleavage the SPO11 catalytic tyrosine remains covalently bound to the target site 5'-end (Neale et al. 2005; Keeney and Kleckner 1995; Pan et al. 2011). Endonucleases, including Sae2 and Mre11, then generate additional DNA backbone cuts 3' to the DSB site that together with exonucleases, cause release of SPO11-oligonucleotide complexes (Garcia et al. 2011; Lam and Keeney 2014; Neale et al. 2005). Purification and sequencing of SPO11-oligonucleotides, which are typically ~20–40 bases in length, has provided a high-

resolution method to profile meiotic DSB patterns genome-wide in fungi and mammals (Pan et al. 2011; Lange et al. 2016; Fowler et al. 2014).

Meiotic DSB and crossover frequency vary extensively along eukaryotic chromosomes and typically concentrate in ~1–2 kilobase hotspots (Baudat et al. 2013; Kauppi et al. 2004; Choi and Henderson 2015). Genetic and epigenetic information make varying contributions to control of hotspot locations and activities in different eukaryotic lineages (Baudat et al. 2013; Kauppi et al. 2004; Choi and Henderson 2015). For example, budding yeast DSB hotspots form predominantly in nucleosome-depleted regions in gene promoters and rarely in exons and terminators (Pan et al. 2011; Lam and Keeney 2015; Wu and Lichten 1994; Fan and Petes 1996). Local base composition, higher-order chromosome structure, transcription factor binding and ATM/ATR kinase signaling have further been shown to modify budding yeast DSB frequency (Lam and Keeney 2014; de Massy 2013; Cooper et al. 2016; Székvölgyi et al. 2015).

In contrast to budding yeast, mouse SPO11-oligonucleotides form at specific C-rich DNA sequence motifs that are bound by the meiotic protein PRDM9, which possesses a zinc finger array and a SET domain that catalyzes histone H3K4^{me3} and H3K36^{me3} (Lange et al. 2016; Mihola et al. 2009; Parvanov et al. 2010; Myers et al. 2010; Baudat et al. 2010; Grey et al. 2011; Brick et al. 2012; Grey et al. 2017; Powers et al. 2016). PRDM9-dependent SPO11 hotspots tend to show well-positioned flanking nucleosomes, which acquire H3K4^{me3} and H3K36^{me3} during meiosis (Grey et al. 2017; Baker et al. 2014; Lange et al. 2016; Brick et al. 2012; Powers et al. 2016). However, H3K4^{me3} levels do not correlate strongly with mouse or yeast SPO11-oligonucleotide levels, implying a downstream role for this chromatin mark (Tischfield and Keeney 2012; Lange et al. 2016). For example, budding yeast H3K4^{me3} is bound by the Spp1 COMPASS complex subunit, which simultaneously interacts with meiotic

chromosome axis protein Mer3 and tethers chromatin loops to repair sites (Sommermeyer et al. 2013; Borde et al. 2009; Acquaviva et al. 2013). Furthermore, the mouse COMPASS subunit CXXC1 interacts with both PRDM9 and the IHO1 axis proteins, suggesting a conserved mechanism of chromatin loop-tethering during DSB repair (Imai et al. 2017).

Plant crossovers are enriched in euchromatin at the chromosome scale, and in proximity to gene promoters and terminators at the fine scale (Choi et al. 2013; Shilo et al. 2015; Drouaud et al. 2013; Wijnker et al. 2013; Horton et al. 2012; Hellsten et al. 2013; Fu et al. 2002; Choulet et al. 2014). Crossovers in plant genomes show positive associations with H3K4^{me3}, histone variant H2A.Z (Choi et al. 2013; Wijnker et al. 2013; Shilo et al. 2015; Drouaud et al. 2013; Liu et al. 2009), A-rich and CTT/CNN-repeat DNA sequence motifs (Shilo et al. 2015; Choi et al. 2013; Wijnker et al. 2013), and can be directly suppressed by acquisition of heterochromatic modifications, such as DNA methylation and H3K9^{me2} (Yelina et al. 2015). However, genome-wide meiotic DSB patterns and their relation to chromatin, DNA sequence and crossover frequency have yet to be reported in a plant genome.

Despite deep conservation of core meiotic factors, such as SPO11, many aspects of genome architecture, chromatin and recombination vary between eukaryotes. For example, budding yeast possesses point centromeres, whereas large, regional centromeres surrounded by repetitive heterochromatin are more common in other eukaryotes (Bloom 2014; Copenhaver et al. 1999; Vincenten et al. 2015; Malik and Henikoff 2009). Equally, although transposable elements are ubiquitous, their diversity and abundance varies between species (Feschotte and Pritham 2007; Beauregard et al. 2008; McClintock 1956). Transposons are typically heterochromatic and show RNA polymerase-II suppression, caused by epigenetic modifications (Slotkin and Martienssen 2007). Repetitive sequences are also frequently crossover-suppressed during meiosis, in order to limit non-allelic homologous recombination

and genome instability (Sasaki et al. 2010). However, evidence exists for specific transposon families promoting meiotic recombination in plants, fungi and animals (Myers et al. 2005; Shi et al. 2010; Sasaki et al. 2013; Horton et al. 2012; Yandeau-Nelson et al. 2005). For example, meiotic gene conversion, although not crossovers, has been observed in maize centromeric transposons (Shi et al. 2010), which indicates DSB formation and interhomolog repair. However, the extent to which plant transposons and repetitive sequences initiate meiotic recombination genome-wide has remained unclear.

To further explore relationships between recombination and chromatin, in genes versus repeats, we mapped meiotic DSBs and crossovers throughout the ~135 megabase *Arabidopsis thaliana* genome, which contains diverse DNA and RNA transposons (Supplemental Fig. S1) (Buisine et al. 2008; Quadrana et al. 2016; Stuart et al. 2016; Kawakatsu et al. 2016; Slotkin and Martienssen 2007). We show that Arabidopsis meiotic DSB hotspots are concentrated in gene promoters, terminators and introns. We also observe strong DSB hotspots inside specific families of DNA transposons, which are enriched within gene regulatory sequences. We show that nucleosome occupancy, driven by AT-sequence richness, is a major determinant of DSB hotspot strength and location in both genes and repeated sequences. Using the *met1* DNA methylation mutant, we demonstrate coordinate epigenetic remodeling of transcription, chromatin and recombination. Activation of meiotic DSBs in *met1* occurs most strongly in centromeric heterochromatin and specific Gypsy and EnSpm/CACTA transposon families. Together, our work reveals both conserved and plant-specific aspects to the meiotic DSB landscape and its relationship to chromatin.

Results

Purification and sequencing of Arabidopsis SPO11-1-oligonucleotides

In order to map meiotic DSBs throughout the Arabidopsis genome we sought to purify and sequence SPO11-1-oligonucleotides (Pan et al. 2011; Grelon et al. 2001). We generated a 6×Myc translational fusion at the C-terminus of Arabidopsis *SPO11-1*, driven by the endogenous promoter, which fully complements *spo11-1* fertility and crossover frequency, measured using fluorescent recombination reporter lines (Fig. 1A–1B and Supplemental Table S1) (Berchowitz and Copenhaver 2008; Grelon et al. 2001). To analyze SPO11-1-Myc during meiosis we performed immunocytology using α-Myc antibodies. SPO11-1-Myc foci were detected from leptotene until pachytene stage, associated with the meiotic chromosome axis, which was visualized by co-immunostaining for the ASYNAPTIC1 (ASY1) HORMA domain protein (Fig. 1C and Supplemental Fig. S2). SPO11-1-Myc foci showed a comparable number (mean=204.6 foci, *n*=10) and duration to those reported for its binding partner MTOPVIB (Fig. 1C and Supplemental Fig. S2) (Vrielynck et al. 2016). No α-Myc signal was detected above background in wild type meiotic cells, or in *SPO11-1-Myc* somatic cells (Fig. 1C). Therefore, SPO11-1-Myc is functional and accumulates on meiotic chromosomes, coincident with endogenous DSB formation (Vrielynck et al. 2016; Sanchez-Moran et al. 2007).

Following protein extraction from meiotic-stage floral buds, SPO11-1-Myc was detectable as a ~54 kDa band using western blotting (Fig. 1D). Oligonucleotides covalently attached to SPO11-1-Myc can be radioactively 3'-end labeled using terminal transferase (Neale and Keeney 2009), which revealed 60–70 kDa complexes (Fig. 1E). No signal was observed when the protocol was repeated without antibody (Fig. 1E). Following proteinase K digestion of SPO11-1-Myc immunoprecipitates and PAGE separation, we detected radiolabelled

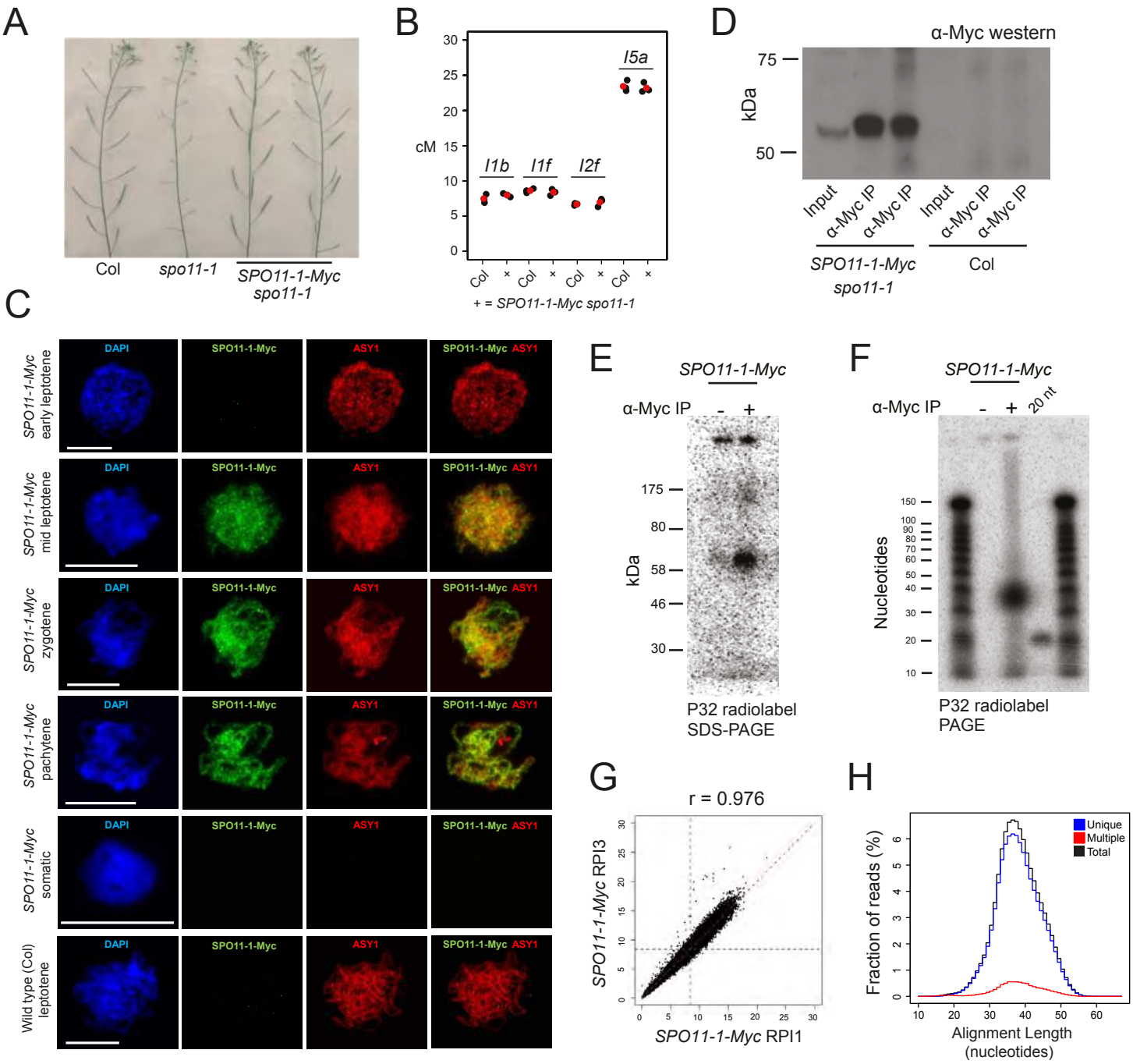

Figure 1. **Purification and sequencing of Arabidopsis SPO11-1-oligonucleotides.** (A) Inflorescences from wild type (Col), *spo11-1* and *SPO11-1-Myc spo11-1* plants. (B) Crossover frequency (cM) measured using fluorescent crossover reporter lines in Col or *SPO11-1-Myc spo11-1*, with mean values in red. (C) Nuclei from *SPO11-1-Myc* or Col pollen mother cells immunostained for α-Myc (green) or α-ASY1 (red), and stained for DAPI (blue). Scale bars=10μM. (D) α-Myc western blotting from *SPO11-1-Myc* or Col extracts, before and after α-Myc immunoprecipitation (α-Myc-IP). (E) Detection of end-radiolabelled SPO11-1-Myc complexes following immunoprecipitation and SDS polyacrylamide gel electrophoresis (SDS-PAGE). (F) Detection of purified SPO11-1-oligonucleotides following proteinase K digestion of immunoprecipitates and polyacrylamide gel electrophoresis (PAGE). A labeled 20 base oligonucleotide (20 nt) was run alongside as a size control. (G) Correlation of SPO11-1 in adjacent 10 kb windows for wild type libraries RPI1 and RPI3 (Supplementary Table 2). Blue dotted lines indicate genome average values. The Pearson's correlation coefficient (*r*) is printed above. (H) Histogram showing lengths of uniquely aligning (blue), multiple-aligning (red) and total (black) SPO11-1 reads.

SPO11-1-oligonucleotides ~35–45 bases in length (Fig. 1F). SPO11-1-oligonucleotides were gel purified and used to generate sequencing libraries, using a protocol adapted from budding yeast (Supplemental Fig. S3) (Pan et al. 2011). Three biological replicate wild type (*SPO11-1-Myc spo11-1*) libraries were sequenced to high depth (11–28 million mapped reads), which showed significant correlation (Fig. 1G, Supplemental Fig. S4 and Supplemental Tables S2–S3). For example, Pearson's *r* between replicates was 0.97–0.98 at the 10 kb scale (Supplemental Table S3). The majority (92.2–93.4%) of SPO11-1-oligonucleotide reads (hereafter called SPO11-1) aligned uniquely, and multiple-mapped reads with equal alignment scores were randomly assigned (Fig. 1H and Supplemental Table S2).

Genomic landscapes of SPO11-1-oligonucleotides, crossovers, euchromatin and heterochromatin

We analyzed SPO11-1 levels in 10 kb windows and plotted DSB frequency throughout the Arabidopsis genome (Fig. 2A–2C). Consistent with broad-scale patterns of crossover recombination (Choi et al. 2013; Giraut et al. 2011; Salomé et al. 2012), SPO11-1 is highest in the euchromatic chromosome arms, lowest in the centromeres (Fig. 2A), and shows a positive correlation with genes (*r*=0.777) and a negative correlation with transposon density (*r*=-0.816). To compare with epigenetic marks, we performed ChIP-seq for the gene-enriched histone modification H3K4^{me3}, which was positively correlated with SPO11-1 (*r*=0.700), whereas centromere-enriched DNA methylation was negatively correlated (*r*=-0.831) (Fig. 2A–2B and Supplemental Table S6) (Yelina et al. 2015). This is consistent with chromatin playing a major role in shaping the Arabidopsis DSB landscape, at the chromosome scale.

In order to compare meiotic DSB levels with the frequency of final crossover products, we used 2,499 crossover events mapped in 363 Col×Ler F_2 plants by genotyping-by-sequencing

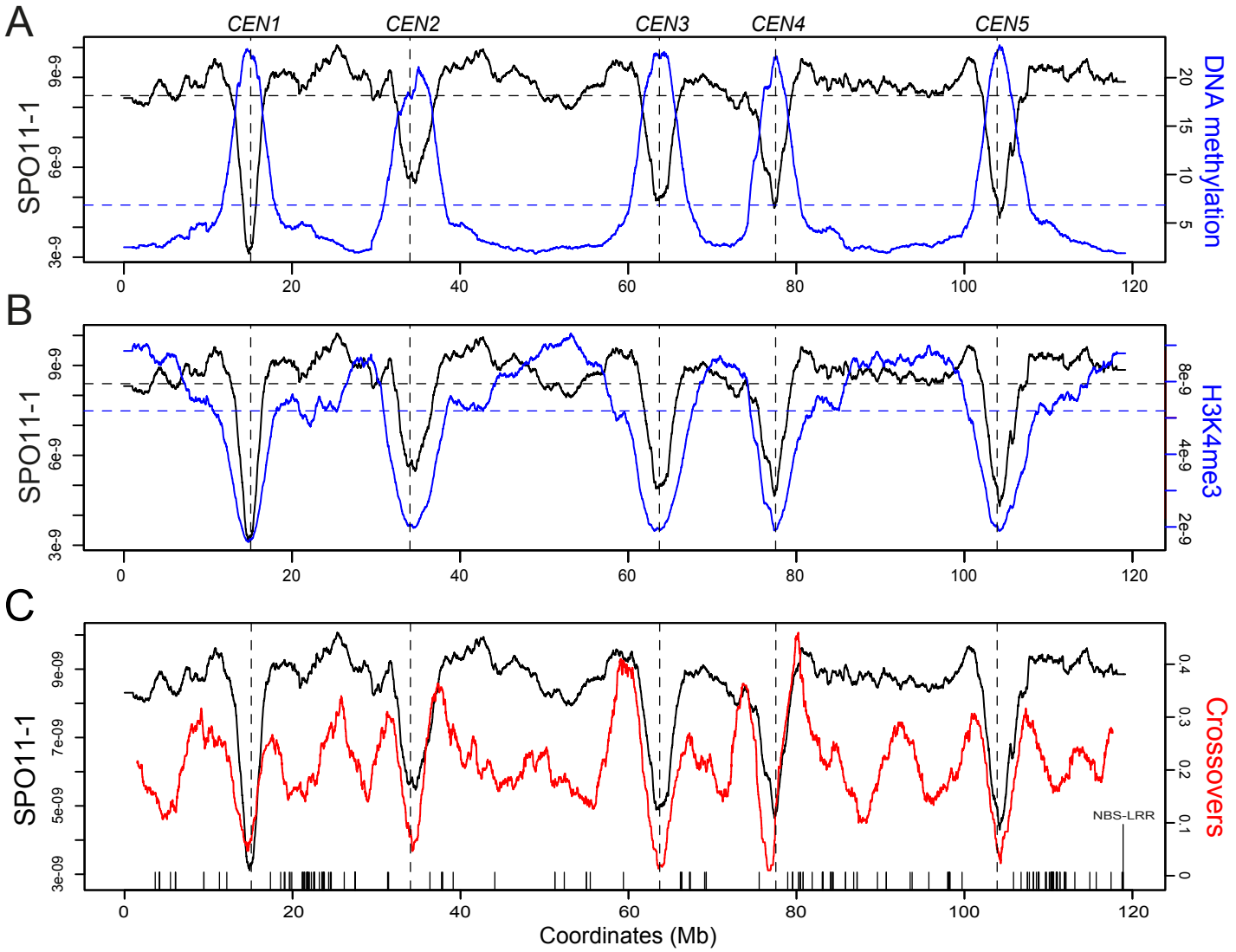

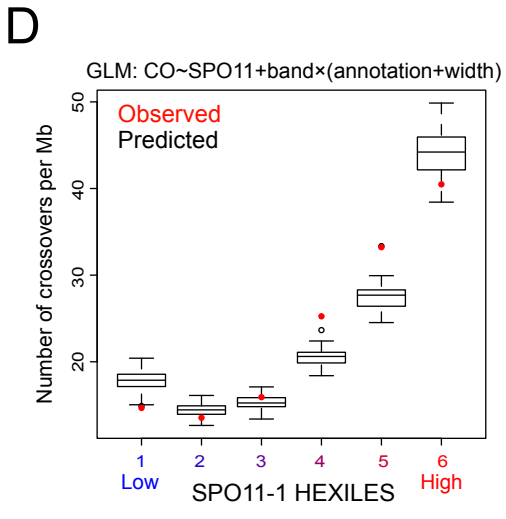

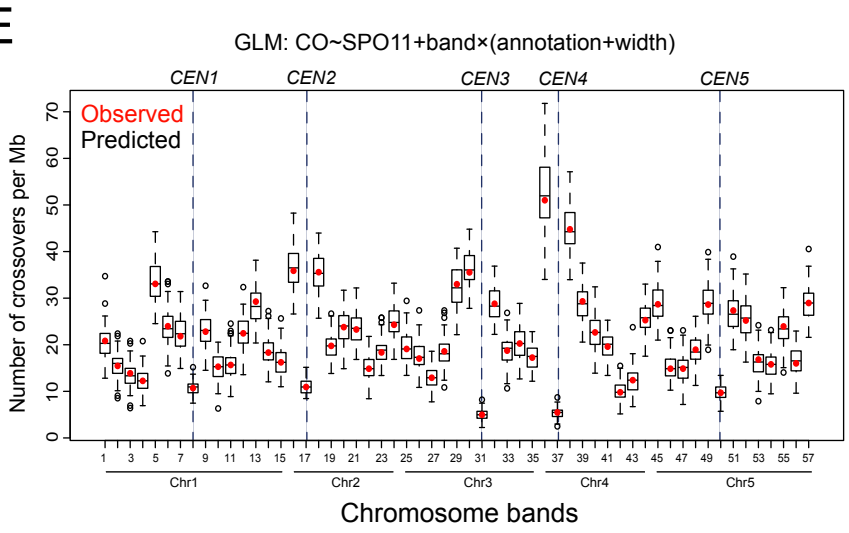

Figure 2. Genomic landscape of SPO11-1 DSBs, crossovers, euchromatin and heterochromatin. (A) SPO11-1 (black) and DNA methylation (blue) density throughout the Arabidopsis genome, with centromeres indicated by vertical dotted lines. Horizontal dotted lines represent mean values. (B) As for (A), but plotting SPO11-1 (black) and H3K4^{me3} (blue). (C) As for (A), but plotting SPO11-1 (black) and crossover frequency (red). Crossovers were identified using genotyping-by-sequencing of Col×Ler F_2 plants. X-axis ticks indicate the positions of NBS-LRR gene homologs. (D) Observed (red dots) crossover overlap per megabase for SNP intervals, grouped according to SPO11-1 hexiles (1=low SPO11-1, 6=high SPO11-1). Boxplots show the range of predicted crossover overlap values based on the generalized linear model (GLM) formula: CO~SPO11+band×(annotation+width). (E) As for (D), but showing observed and predicted crossover overlaps per megabase, according to two megabase chromosomal bands.

(Fig. 2C–2E and Supplemental Table S4) (Choi et al. 2016; Rowan et al. 2015). Crossovers were mapped between Col/Ler SNPs to a mean resolution of 970 bp. At the chromosome scale there was a positive correlation between SPO11-1 and crossover frequency (r=0.593) (Fig. 2C). However, there was also significant variation in the ratio of SPO11-1 to crossovers along the chromosome arms (Fig. 2C), which may reflect modification of recombination downstream of DSB formation, for example by polymorphism, or additional features of chromosome architecture. We used a logistic model to analyze the likelihood of observing crossovers relative to other genome features. This revealed a strong positive effect for SPO11-1 levels (10.87, P=9.36×10^{-87}), with weaker but significant effects for chromosome position and sequence annotation (Fig. 2D–2E and Supplemental Table S5). Therefore, overall higher levels of initiating meiotic DSBs associate with higher final crossover levels.

SPO11-1 DSB hotspots in nucleosome-depleted gene regulatory regions

Budding yeast meiotic DSB hotspots occur in nucleosome-depleted regions within gene promoters (Pan et al. 2011; Lam and Keeney 2015; Wu and Lichten 1994; Fan and Petes 1996; Nicolas et al. 1989), whereas mammalian PRDM9-dependent DSB hotspots tend to be located intergenically at specific C-rich sequence motifs (Myers et al. 2008; Brick et al. 2012; Kong et al. 2010; Lange et al. 2016). Therefore, we analyzed Arabidopsis SPO11-1-oligonucleotides in relation to gene transcriptional start sites (TSSs) and termination sites (TTS) (Fig. 3A–3B). We also analyzed nucleosome occupancy by performing micrococcal nuclease digestion of chromatin, followed by sequencing of mononucleosomal DNA (MNase-seq) (Fig. 3A–3B and Supplemental Table S7) (Choi et al. 2016). Similar to budding yeast, SPO11-1 was highest in Arabidopsis nucleosome-free regions located in gene promoters (Fig. 3A–3C). Interestingly we also observe strong DSB hotspots in nucleosome-free terminators, where plant crossover hotspots are also observed (Fig. 3A–3C) (Choi et al. 2013; Wijnker et al. 2013). A further difference is that Arabidopsis genes possess on average

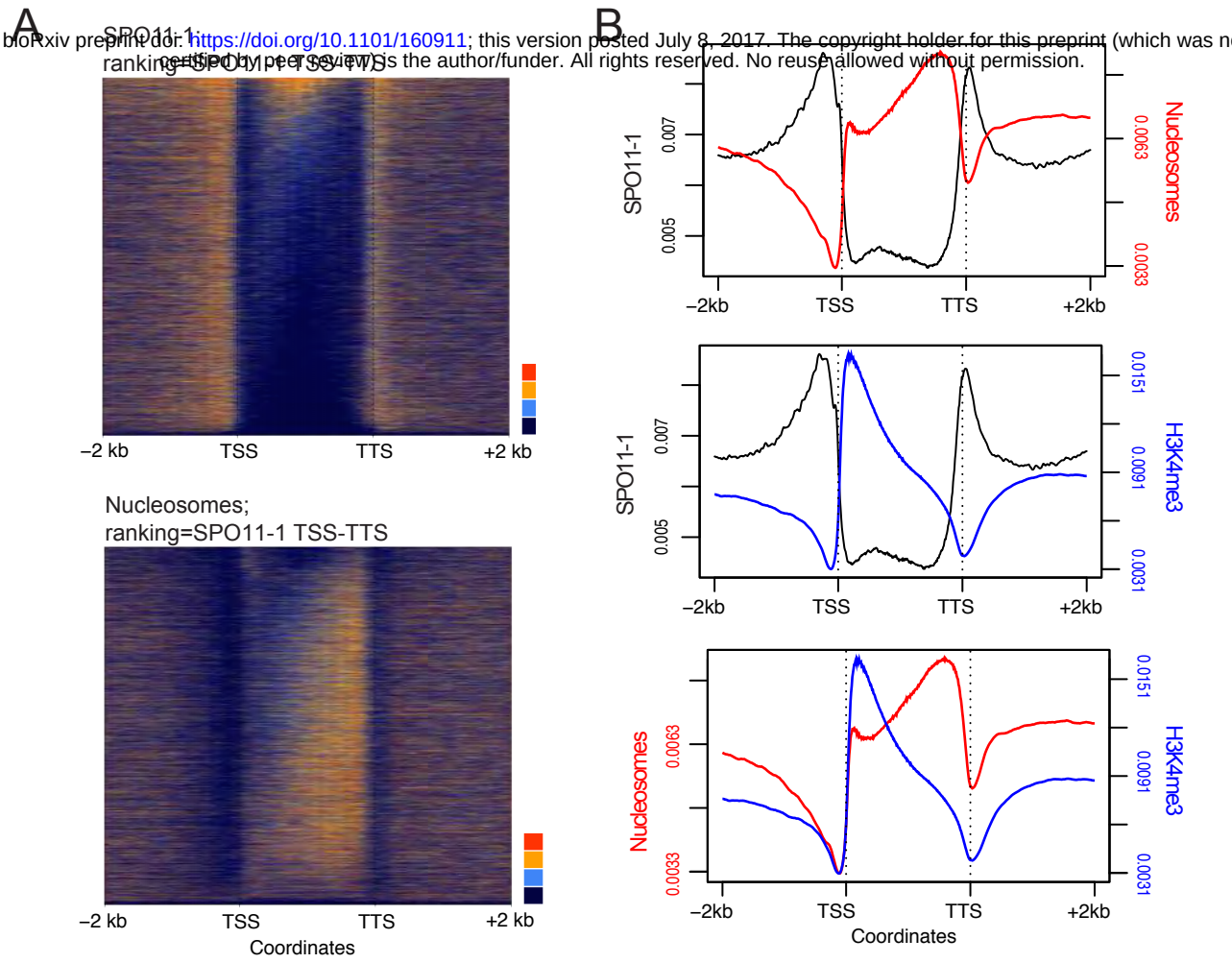

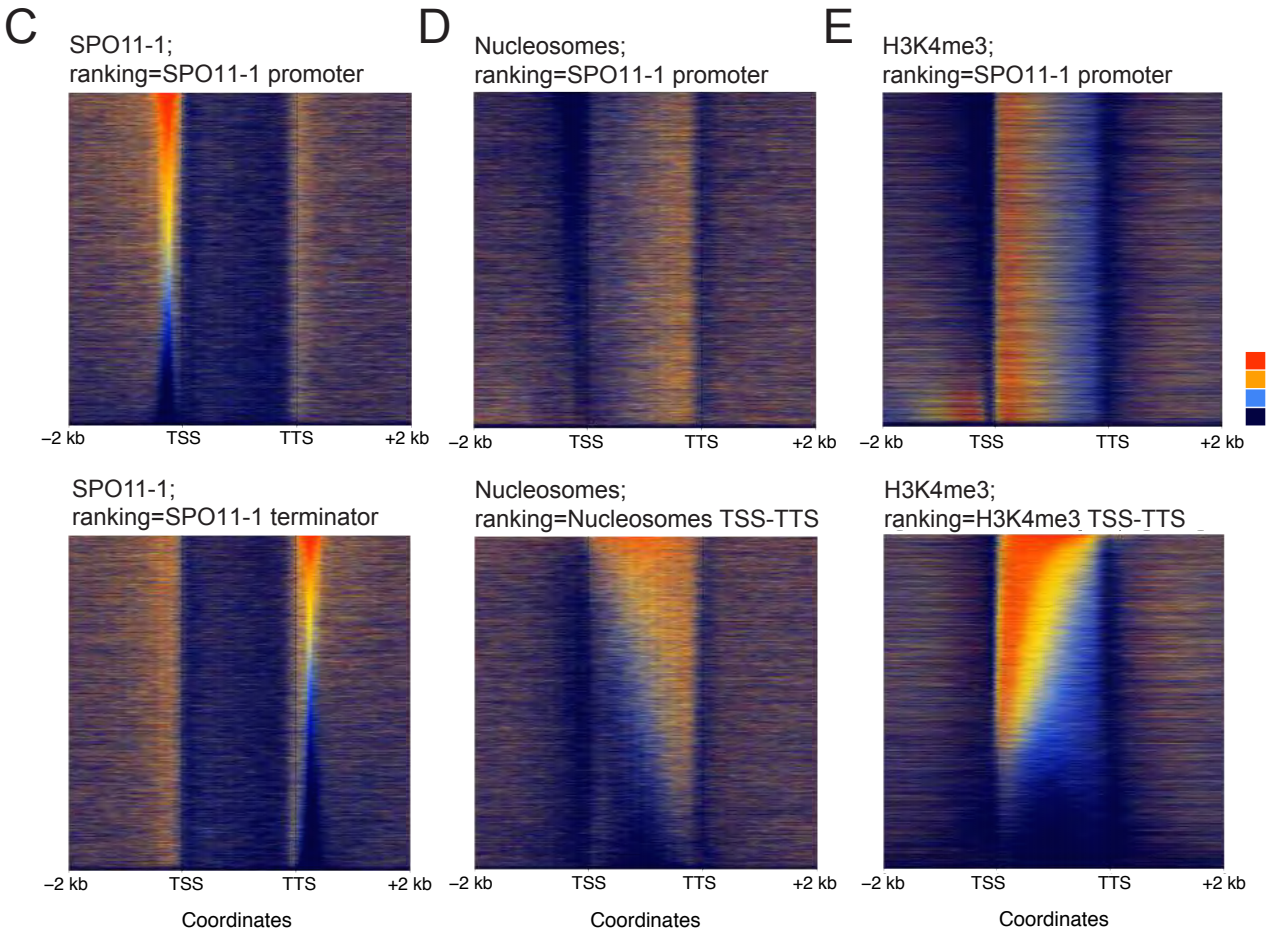

Figure 3. SPO11-1 DSB hotspots in gene promoter and terminator nucleosome-free regions. (A) Heat maps of SPO11-1-oligonucleotides (upper) and nucleosomes (lower) within gene transcriptional units (between transcriptional start (TSS) and termination (TTS) sites) and 2 kb flanking regions. Each row represents an individual gene, which have been ordered by SPO11-1-oligonucleotide normalized coverage values between TSS and TTS. SPO11-1 and nucleosome values equal to defined quantiles were mapped linearly to a vector of six colors (dark blue (lowest), blue, light blue, yellow, orange, red (highest)). (B) Density of SPO11-1-oligonucleotides (black), nucleosome occupancy (MNase-seq, red), or H3K4^{me3} (ChIP-seq, blue) in wild type, across gene transcriptional units (TSS to TTS) and in flanking 2 kb windows. (C) Heat maps as for (A), but showing SPO11-1 ranked by SPO11-1 levels in gene promoters (upper, -500 bp upstream of TSS) or gene terminators (lower, +500 bp downstream of TTS). (D) Heat maps as for (A), but showing nucleosomes ranked by SPO11-1 levels in gene promoters (upper) or by nucleosomes within TSS–TTS (lower). (E) Heat maps as for (A), but showing H3K4^{me3} ranked by SPO11-1 levels in gene promoters (upper) or by H3K4^{me3} within TSS–TTS (lower).

6.7 exons (Cheng et al. 2017), whereas budding yeast genes lack introns (Pan et al. 2011). We observe that Arabidopsis introns have higher SPO11-1 and lower nucleosomes compared with exons (Supplemental Fig. S5B–S5D). However, SPO11-1 is overall suppressed within relatively nucleosome-occupied gene bodies, compared with flanking nucleosome-depleted promoter and terminator regions (Fig. 3A–3C and Supplemental Fig. S5A). As expected, H3K4^{me3} shows prominent enrichment at the +1 nucleosome position, immediately downstream of TSS, within gene bodies (Fig. 3B) (Zhang et al. 2009).

To investigate control of DSB levels we ranked genes according to SPO11-1 in 500 bp windows upstream of gene TSS (promoters), or downstream of TTS (terminators) (Fig. 3C). Levels of promoter SPO11-1 did not strongly associate with terminator levels, showing that meiotic DSBs vary independently at opposite ends of genes (Fig. 3C). We used the SPO11-1 promoter ranking to look at associated variation in nucleosome occupancy (MNase) and H3K4^{me3} levels. High SPO11-1 promoters strongly associate with lower promoter nucleosome occupancy, consistent with DNA accessibility being a major determinant of Arabidopsis DSB levels (Fig. 3D). In contrast, H3K4^{me3} levels within genes did not show a strong association with promoter SPO11-1 levels (Fig. 3E). This supports a recombination-promoting role for H3K4^{me3} downstream of DSB formation, consistent with analysis of mouse and budding yeast SPO11-oligonucleotides (Tischfield and Keeney 2012; Lange et al. 2016).

SPO11-1 hotspots and coldspots in transposable elements

To explore meiotic DSB levels within repetitive sequences we selected 29,150 transposable elements from 10 DNA and RNA families for analysis (Supplemental Fig. S1 and Supplemental Table S8) (Buisine et al. 2008). Extensive SPO11-1 variation was observed between transposon families, with high DSB levels in Helitrons, which transpose via rolling-circle replication, and Pogo/Tc1/Mariner and MuDR ‘cut-and-paste’ DNA transposons (Fig.

4A and Supplemental Table S8) (Kapitonov and Jurka 2001; Slotkin and Martienssen 2007). In contrast, retrotransposons that replicate via RNA intermediates, including LTR and non-LTR families, were SPO11-1 coldspots (Fig. 4A and Supplemental Table S8) (Beauregard et al. 2008). As observed for genes (Fig. 3), variation in transposon family SPO11-1 negatively correlated with nucleosome occupancy (r=-0.96) (Fig. 4B and Supplemental Table S8). We divided transposons into six groups (hexiles) after ranking by within element SPO11-1 levels (Figure 4C; hexile 1=highest, hexile 6=lowest). This grouping showed strong correlations between higher SPO11-1 and reduced transposon lengths (r=-0.80), lower nucleosome occupancy (r=-0.94), greater DNA (r=0.95) and fewer RNA transposons (r=-0.95) (Fig. 4C and Supplemental Tables S8-S9). At the chromosome scale, high SPO11-1 transposons (e.g. Helitrons and Pogo/Tc1/Mariner) show elevated density in the chromosome arms and pericentromeres, whereas low SPO11-1 transposons (e.g. Gypsy LTR) are centromere-enriched (Fig. 4D). Differences in DSB activity between transposon families are also evident locally, for example comparing a nucleosome-dense retroelement coldspot *ATCOPIA4* with an adjacent cluster of nucleosome-depleted Helitron hotspots (Fig. 4E–4F). Many DSB hotspot DNA transposons are short, non-autonomous fragments, although high SPO11-1 was also observed within full length Helitron and *Lemi1* Pogo transposons (Supplemental Fig. S6A–S6D) (Feschotte and Mouchès 2000; Kapitonov and Jurka 2001). Hence, despite the expectation that transposons would be suppressed for meiotic DSBs, we observe that specific families of repetitive elements are nucleosome-depleted SPO11-1 hotspots.

Nucleosomes, DNA sequence and SPO11-1 within genes and transposons

To further investigate spatial relationships between meiotic DSBs, chromatin and DNA sequence, we analyzed 4 kb windows around gene TSS and TTS, or transposon start and end coordinates, each according to SPO11-1 hexile groups (Fig. 5A–5B and Tables S9–S11). Again, a strong negative relationship between SPO11-1 and nucleosome occupancy

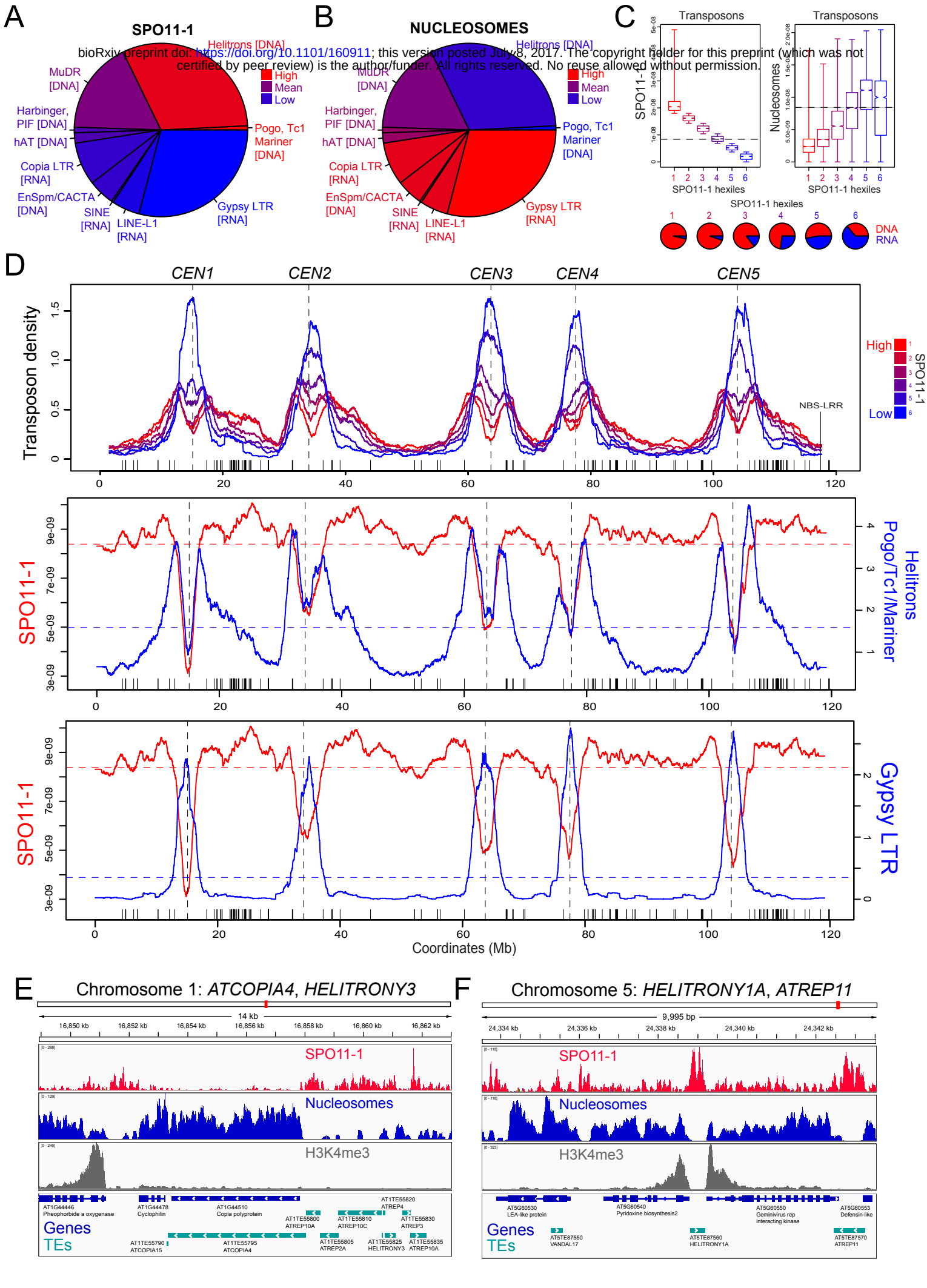

Figure 4. **Meiotic recombination and chromatin variation between Arabidopsis transposons.** (A) Pie chart showing Arabidopsis transposon families, with slice size proportional to physical length, and color-coded according to SPO11-1 levels. The color equivalent to the genome-wide mean value is inset. (B) As for (A), but showing nucleosome occupancy (MNase-seq). (C) Box plots showing SPO11-1 and nucleosome occupancy, according to transposon SPO11-1 hexile groups, with horizontal lines indicating the genome average value. Inset pie charts show the proportion of DNA (red) and RNA (blue) transposons for each SPO11-1 hexile. (D) Density of transposons through the Arabidopsis genome according to SPO11-1 hexile (red=highest SPO11-1, blue=lowest SPO11-1). X-axis ticks indicate NBS-LRR gene homologs. Plotted beneath are SPO11-1 (red) versus Helitron/Pogo/Tc1/Mariner class DNA transposons (blue), or Gypsy RNA transposons (blue). (E)–(F) Close-ups of chromosomal regions showing SPO11-1 (red), nucleosomes (blue) and H3K4^{me3} (grey) density, relative to gene (dark blue) and transposon (light blue) annotation shown beneath. Note in (F), the presence of a *DEFENSIN* gene At5g60553 associated with a Helitron *ATREP11* hotspot.

was observed in both genes and transposons (Fig. 5A–5B and Supplemental Tables S9–S11). In the high SPO11-1 regions, we also observe quantitative enrichment of AT-rich sequence motifs that have previously been associated with high crossovers (Fig. 5A–5B and Supplemental Tables S6–S8) (Horton et al. 2012; Choi et al. 2013; Shilo et al. 2015; Wijnker et al. 2013). As AT-sequence richness is known to exclude nucleosomes (Segal and Widom 2009), we propose that these motifs cause higher SPO11-1 accessibility via this effect, leading to higher DSB formation and crossover frequency (Fig. 5A–5B).

We also note that high SPO11-1 genes and transposons show close proximity to one another (Fig. 5A–5B). Helitron transposons are known to insert into AT dinucleotides (Kapitonov and Jurka 2001), and *Lemi1* Pogo transposons insert into TA dinucleotides (Guermonprez et al. 2008). Therefore, transposon integration site preference likely contributes to DNA element enrichment in AT-rich gene promoters and terminators, where they further contribute to nucleosome exclusion and high meiotic DSB levels (Fig. 5A–5B). High recombination rates may also provide an explanation for the tendency of DSB hotspot transposons to be shorter (Supplemental Tables S8–S9), due to promotion of non-homologous recombination and sequence rearrangement (Sasaki et al. 2010). Together, these findings reveal intimate connections between DNA sequence, chromatin and recombination around Arabidopsis genes and transposons.

Meiotic DSB hotspot transposons are enriched in proximity to immunity genes

To investigate genes associated with high DSB levels, we tested for enrichment of Gene Ontology (GO) terms, following ranking by promoter SPO11-1 levels (Fig. 3C). This revealed a strong association with biotic defense GO terms (Supplemental Table S12), which was driven by high recombination *DEFENSIN* genes (Supplemental Fig. S6E–S6F). *DEFENSINS* encode small cysteine-rich peptides with roles in antimicrobial defense and pollen-pistil

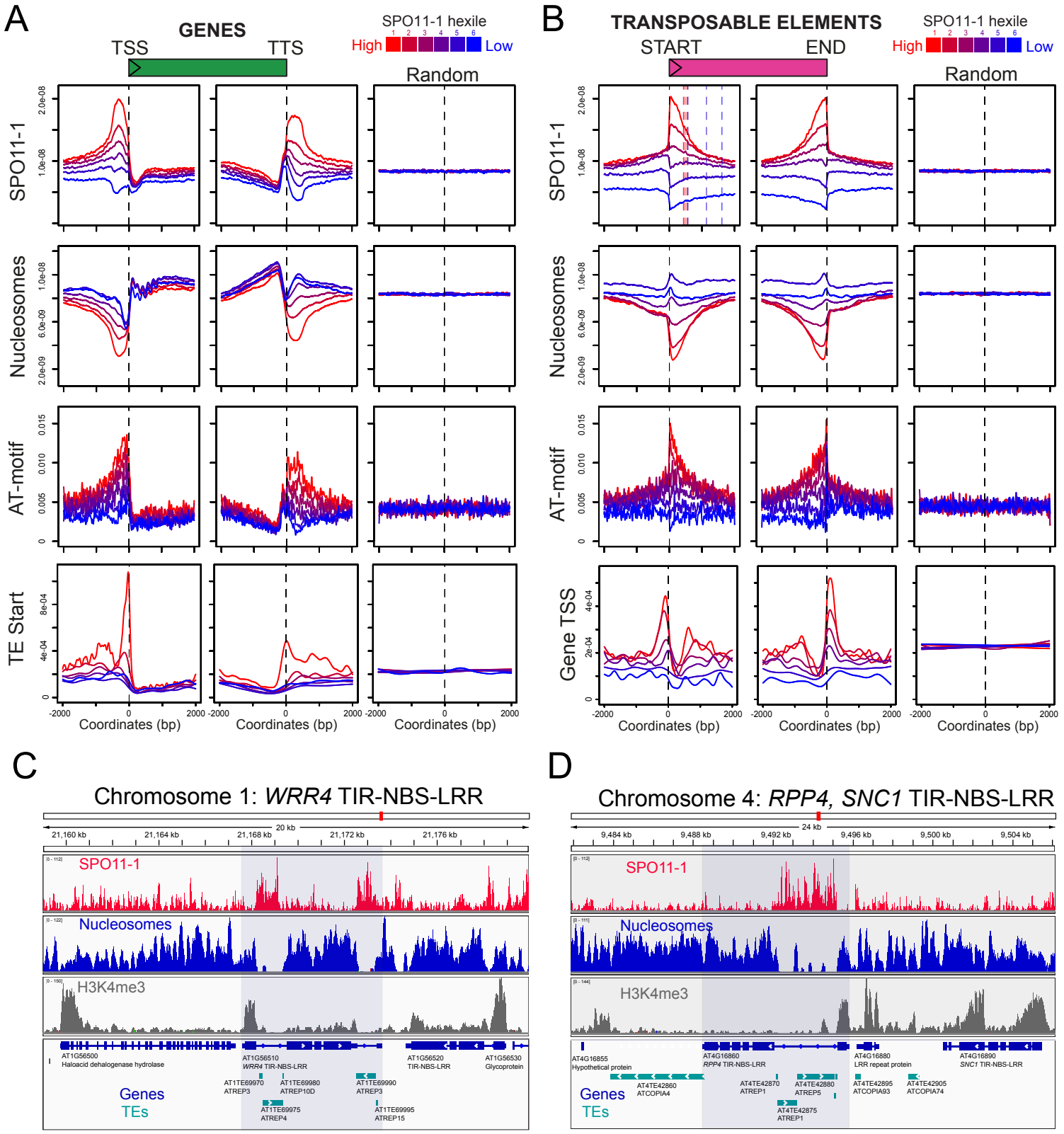

Figure 5. **Nucleosomes, AT-sequence motifs and SPO11-1 DSBs within genes and transposons.** (A) Density of SPO11-1, nucleosomes, AT-motifs (Choi et al. 2013), and TE start coordinates in 4 kb windows around gene transcriptional start sites (TSSs) or termination sites (TTSs), or the same number of random (Random) positions. Genes are grouped according to SPO11-1 promoter or terminator hexiles (red=highest, blue=lowest). (B) As for (A) but analyzing transposon SPO11-1 hexiles, and showing gene TSS proximity. (C) Close-ups of chromosomal regions showing SPO11-1 (red), nucleosomes (blue) and H3K4^{me3} (grey), relative to gene (dark blue) and transposon (light blue) annotations. The *WRR4* TIR-NBS-LRR resistance gene is highlighted which contains transposon hotspots within its introns. (D) As for (C), with the *RPP4* TIR-NBS-LRR resistance gene highlighted, which contains intronic hotspot transposons.

interactions (Silverstein et al. 2005). Further association of recombination hotspots and immunity genes is evident at the chromosome scale, where high SPO11-1 transposons show elevated density within the nucleotide binding site-leucine rich repeat (NBS-LRR) immune gene clusters on the right arms of chromosomes 1 and 5 (Fig. 4D) (Choi et al. 2016), and 73 of 197 NBS-LRR genes are within 500 base pairs of DSB hotspot transposons (Supplemental Table S13). For example, the NBS-LRR crossover hotspots *RAC1* and *HRG1* are flanked by Helitron and MuDR hotspot transposons, respectively (Supplemental Fig. S6G–S6H and Supplemental Table S13) (Choi et al. 2016). Further examples include the *RPP4* and *WRR4* oomycete resistance genes, which contain strong *ATREP* Helitron DSB hotspots within their introns (Fig. 5C–5D and Supplemental Table S13) (van der Biezen et al. 2002; Borhan et al. 2008). As Arabidopsis NBS-LRR genes are sites of natural structural diversity and DNA methylation polymorphism in populations (Kawakatsu et al. 2016; Quadrana et al. 2016; Stuart et al. 2016), we propose that gene-proximal DNA transposons may act as meiotic recombination enhancers, contributing to the high levels of genetic and epigenetic variation observed at these loci.

Epigenetic remodeling of SPO11-1 DSBs, chromatin and transcription in *met1* DNA methylation mutants

Heterochromatic marks, such as DNA methylation, play critical roles in transcriptionally silencing transposable elements and thereby limiting their proliferation within eukaryotic genomes (Slotkin and Martienssen 2007). To directly investigate the role of heterochromatin on transposon recombination, chromatin and transcription, we compared SPO11-1, nucleosomes, H3K4^{me3} and RNA expression genome-wide in wild type and *met1*. *MET1* encodes the major CG sequence context maintenance DNA methyltransferase in Arabidopsis (Stroud et al. 2013; Saze et al. 2003; Kankel et al. 2003). In *met1* mutants cytological decondensation of heterochromatin occurs, together with elevated transposon

452 transcription and mobility (Mathieu et al. 2007; Saze et al. 2003; Kato et al. 2003). We
453 therefore sought to test whether related changes in heterochromatic meiotic DSBs occur in
454 *met1*. For all experiments we used the null *met1-3* allele, which was isolated in a Columbia
455 background (Saze et al. 2003).
456
457 At the chromosome-scale *met1-3* shows pronounced loss of CG DNA methylation within the
458 centromeric regions (Stroud et al. 2013). We observe that this is mirrored by an increased
459 centromeric SPO11-1 differential between *met1* and wild type (ΔSPO11-1) (Fig. 6A). The
460 *met1* ΔSPO11-1 differential also strongly negatively correlates with the *met1* nucleosome
461 differential (r=-0.879), and positively with the *met1* H3K4^{me3} differential (P=0.837) (Fig. 6A).
462 This shows that loss of CG DNA methylation causes broad-scale gain of both meiotic
463 SPO11-1 DSBs and euchromatic chromatin states (reduced nucleosome occupancy and
464 increased H3K4^{me3}) within the *met1* centromeric regions. Regions showing high *met1*
465 ΔSPO11-1 differential also strongly correlate with the densities of Gypsy (r=0.913) and
466 EnSpm/CACTA (r=0.892) transposons, which are SPO11-1 coldspots in wild type (Figs. 4A
467 and 6A).
468
469 To analyze changes in recombination at the fine-scale, we compared SPO11-1 levels within
470 transposons between wild type and *met1* (Fig. 6B). 12,224 transposons (41.9%) showed net
471 gain of SPO11-1 in *met1* (Fig. 6B). These recombination-activated transposons also show
472 significantly reduced nucleosome occupancy, elevated H3K4^{me3} and increased transcription
473 in *met1* (ANOVA all P=<2.50×10^{-6}) (Fig. 6B). This is consistent with the trends observed at
474 chromosome scale, and demonstrate that loss of CG methylation causes transposons to gain
475 euchromatic features and increase meiotic recombination initiation. These trends are also
476 evident at specific transposable elements. For example, the *ATENSPM9* and *ATENSPM10*
477 EnSpm/CACTA and *ATGP3* Gypsy transposons show coordinate activation of transcription

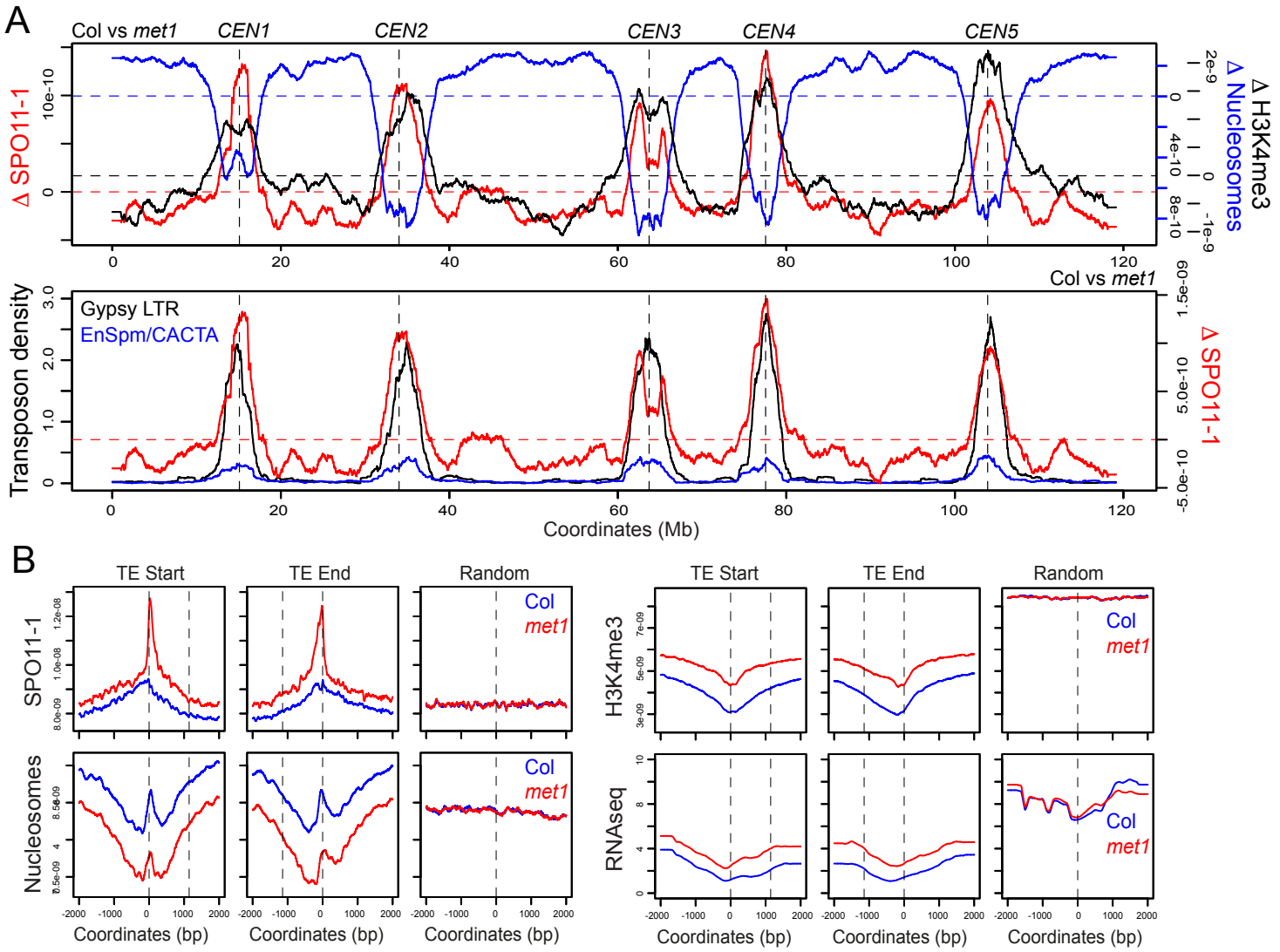

Figure 6. **Coordinate epigenetic remodeling of chromatin, transcription and meiotic DSBs in *met1* DNA methylation mutants.** (A) Differential (Δ) signal of SPO11-1 (red), nucleosomes (blue) and H3K4^{me3} (black) in *met1* compared with wild type (Col), throughout the Arabidopsis genome. Horizontal dotted lines indicate zero differential. Centromeres are indicated by vertical dotted lines. The lower plot shows ΔSPO11-1 (red) compared with Gypsy (black) and EnSpm/CACTA (blue) transposon densities. (B) SPO11-1, nucleosomes, H3K4^{me3} or RNAseq data in Col (blue) versus *met1* (red), analyzed in 4 kb windows around the start and end of those transposons with positive ΔSPO11-1 values (n=12,224), or the same number of random positions. The mean width of TEs analyzed is indicated by the vertical dotted lines.

and meiotic DSBs in *met1*, in addition to showing reduced nucleosome occupancy and gain of H3K4^{me3} (Fig. 7A).

To further analyze the interaction of chromatin structure and meiotic DSBs, we identified 74,401 highly positioned nucleosomes in wild type from our MNase-seq data. Of these positions 30,276 showed reduced nucleosome occupancy in *met1* (Fig. 7B). These nucleosome positions show high CG methylation in wild type, with peak ^{m}CG levels immediately flanking the central nucleosomal peak (Fig. 7C). In *met1*, CG methylation is lost at these positions, which is coincident with significantly reduced nucleosome occupancy and increased SPO11-1 DSBs (ANOVA all P=<2.2×10^{-16}) (Fig. 7B). Taken together, this demonstrates coordinate remodeling of chromatin, histone modifications, transcription and meiotic recombination, caused by loss of CG DNA methylation in *met1*. Epigenetic remodeling of *met1* recombination is evident at the scale of chromosomes, transposons and individual nucleosomes.

A

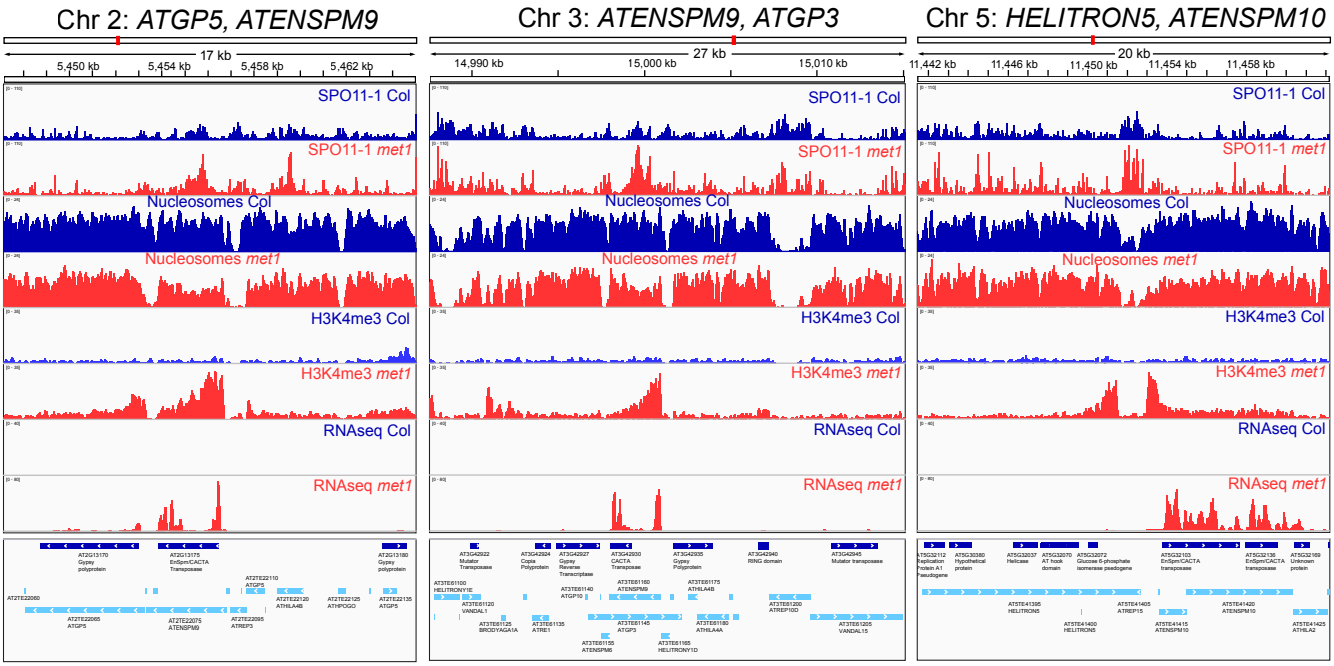

B

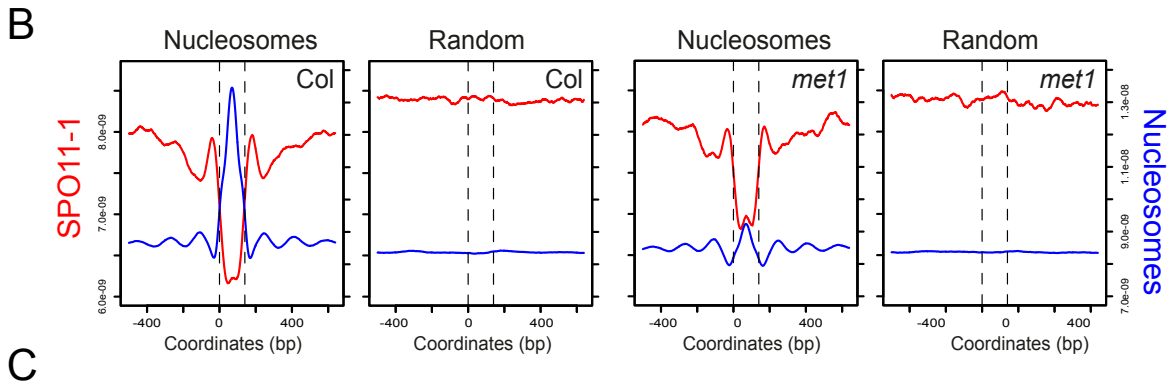

C

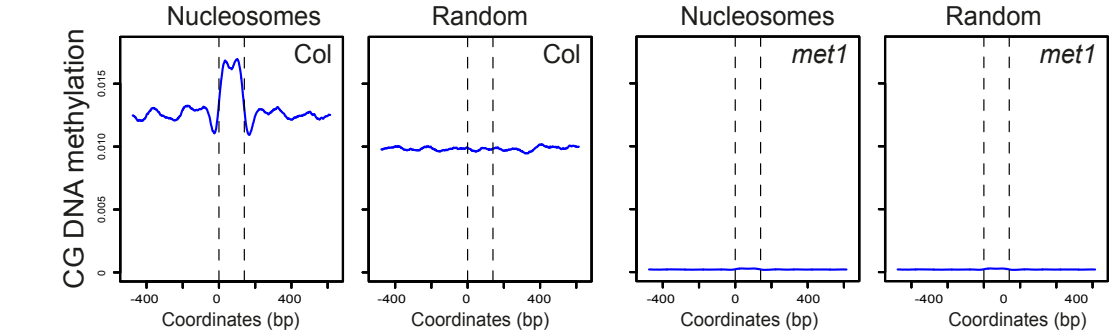

Figure 7. Fine-scale epigenetic remodeling of *met1* transposon chromatin, transcription and recombination. (A) Close-up of chromosomal regions showing SPO11-1, nucleosomes, H3K4^{me3} and RNAseq data, relative to gene (dark blue) and transposon (light blue) annotation, for Col (blue) and *met1* (red). (B) Plots analyzing SPO11-1 (red) and nucleosomes (blue) in Col and *met1* for highly positioned nucleosomes that are differentially occupied in *met1* (n=30,267), or the same number of random positions. (C) As for (B), but analyzing CG DNA methylation (blue) in wild type and *met1*.

Discussion

The Arabidopsis meiotic DSB landscape shows both conserved and plant-specific features, compared with SPO11-oligonucleotide maps generated in fungal and mammalian species (Pan et al. 2011; Lange et al. 2016; Fowler et al. 2014). Consistent with the absence of PRDM9 in plants and fungi, Arabidopsis hotspots are more similar to those observed in budding yeast promoters, which are driven by nucleosome occupancy (Pan et al. 2011; Lam and Keeney 2015; Wu and Lichten 1994; Fan and Petes 1996). However, Arabidopsis also shows SPO11-1 hotspots within nucleosome-depleted gene terminators and introns, indicating that varying gene architectures can influence meiotic DSB patterns between species. Interestingly, avian crossover hotspots are also observed at both gene promoters and terminators (Singhal et al. 2015), meaning that recombination hotspots located at gene 3'-ends may be widely conserved.

Consistent with analysis of yeast and mouse SPO11-oligonucleotides, we do not observe a strong relationship between H3K4^{me3} and DSB levels (Tischfield and Keeney 2012; Lange et al. 2016). However, as this modification correlates positively with plant crossover frequency (Choi et al. 2013; Liu et al. 2009; Shilo et al. 2015), it is likely that H3K4^{me3} plays a recombination-promoting role downstream of DSB formation, potentially via tethering repair sites to the chromosome axis, as in budding yeast and mammals (Sommermeyer et al. 2013; Borde et al. 2009; Acquaviva et al. 2013; Imai et al. 2017). No evidence for PRDM9-like proteins exist in plants, which acts to direct recombination hotspots to specific sequence motifs in mammals (Lange et al. 2016; Mihola et al. 2009; Parvanov et al. 2010; Myers et al. 2010; Baudat et al. 2010; Grey et al. 2011; Brick et al. 2012; Grey et al. 2017). However, we observe a strong influence of AT-sequence richness on SPO11-1 levels. As AT-richness excludes nucleosomes (Segal and Widom 2009), we propose that these motifs allow

578 increased SPO11-1 access to DNA, and this underlies their association with elevated
579 crossover frequency (Shilo et al. 2015; Choi et al. 2013; Wijnker et al. 2013).
580
581 Several additional differences are notable between the budding yeast and Arabidopsis
582 genomes when comparing their DSB landscapes. First is the possession of point versus
583 regional centromeres (Bloom 2014; Copenhaver et al. 1999; Vincenten et al. 2015), and that
584 Arabidopsis contains a larger and more diverse transposon complement (Buisine et al. 2008;
585 Quadrana et al. 2016; Stuart et al. 2016). Arabidopsis transposons are enriched in
586 pericentromeric heterochromatin and are transcriptionally silenced by DNA methylation
587 (Saze et al. 2003; Kato et al. 2003), which is a chromatin modification not present in budding
588 or fission yeast. Using the *met1* mutant we show that loss of maintenance of CG DNA
589 methylation causes coordinated gain of euchromatic marks, transcription and SPO11-1
590 DSBs within Arabidopsis centromeric regions. Gain of meiotic DSBs in *met1* was greatest in
591 coldspot transposons, including the EnSpm/CACTA and Gypsy families. Hence, DNA
592 methylation simultaneously silences transcription and initiation of meiotic recombination in
593 specific families of Arabidopsis transposons. This finding is reminiscent of increased SPO11-
594 DSBs detected in specific retrotransposon classes in mouse *dnmt3l* DNA methylation
595 mutants (Zamudio et al. 2015), indicating that epigenetic silencing of transposon
596 recombination is a conserved feature of plant and mammalian genomes.
597
598 Despite the expectation that transposons would be recombination-suppressed, in order to
599 avoid genome instability (Sasaki et al. 2010), we show that specific Arabidopsis DNA
600 transposons contain strong meiotic DSB hotspots. These DNA transposons are AT-rich and
601 nucleosome-depleted in wild type and frequently occur in close proximity to genes. As
602 Helitrons and Pogo/Tc1/Mariner transposons display TA and AT dinucleotide insertion site
603 preferences (Guermonprez et al. 2008; Kapitonov and Jurka 2001), this likely contributes to

604 their enrichment in AT-rich gene regulatory regions, where they may further contribute to
605 nucleosome exclusion and enhanced SPO11-1 DSB levels. Higher meiotic recombination
606 initiation may also be responsible for DSB hotspot transposons tending to occur as shorter,
607 non-autonomous fragments. For example, insertions, deletions and rearrangements can
608 result from non-allelic recombination between repeated loci (Sasaki et al. 2010). Together,
609 these data reveal unexpected diversity in the chromatin and recombination landscapes
610 between Arabidopsis transposable element families. As plant genomes vary greatly in the
611 abundance and chromosomal distributions of specific transposon families (Buisine et al.
612 2008; Choulet et al. 2014; Guermonprez et al. 2008; Kapitonov and Jurka 2001; Quadrana et
613 al. 2016; Stuart et al. 2016; Liu et al. 2009), repetitive elements may contribute to diversity of
614 meiotic recombination patterns between species.
615
616 A role for transposons modifying transcription in proximity to genes is well established,
617 consistent with Barbara McClintock's 'Controlling Elements' concept (Slotkin and
618 Martienssen 2007; McClintock 1956). Here we demonstrate that transposons also shape the
619 meiotic DSB and chromatin landscape, within Arabidopsis gene regulatory regions. We
620 propose that nucleosome-depleted SPO11-1 hotspot transposons may provide an adaptive
621 function within plant genomes, by acting as recombination-enhancers. This may be
622 particularly important at the diverse NBS-LRR resistance gene family, which participate in
623 host-pathogen coevolution (Jones and Dangl 2006). Interestingly, these immune loci are also
624 known regions of high genetic and epigenetic divergence between Arabidopsis populations
625 (Alonso-Blanco et al. 2016; Kawakatsu et al. 2016). We propose that hotspot transposons
626 directly contribute to this diversity by recruiting SPO11-1-dependent DSBs during meiosis.
627 Together, our work reveals novel mechanisms whereby mobile genetic elements can
628 influence meiotic recombination, chromatin, diversity and adaptation in their host genomes.
629

Methods

Generation of Arabidopsis *SPO11-1-Myc spo11-1* lines

Six c-Myc (6xMyc) epitopes were translationally fused to a genomic clone of the *SPO11-1* gene in the pPZP211 binary vector, which was transformed into wild type Arabidopsis (Col-0) using *Agrobacterium tumefaciens* strain GV3101, via floral dipping. *SPO11-1-Myc* transformants were crossed with *spo11-1-3* (SALK_146172) heterozygotes to perform fertility complementation tests(Hartung et al. 2007).

Recombination measurements using fluorescent seed and pollen

Crossover measurements using fluorescent seed or pollen were carried out as described(Ziolkowski et al. 2015; Yelina et al. 2013).

Immunocytological analysis

Chromosome spreads of Arabidopsis pollen mother cells and immunostaining of ASY1 and SPO11-1-Myc were performed using fresh buds, as described(Armstrong et al. 2002). The following antibodies were used: α-ASY1(Armstrong et al. 2002), (rabbit, 1/500 dilution), α-Myc (9E10, Santa Cruz Biotechnology) (mouse, 1/50 dilution). Microscopy was conducted using a DeltaVision Personal DV microscope (Applied precision/GE Healthcare) equipped with a CDD Coolsnap HQ2 camera (Photometrics). Image capture and analysis was performed using SoftWoRx software version 5.5 (Applied precision/GE Healthcare).

Immunoprecipitation of SPO11-1-oligonucleotide complexes

Approximately 30 grams of *SPO11-1-Myc spo11-1-3* floral buds were ground to a fine powder in liquid nitrogen and resuspended in 4 volumes of lysis buffer (25 mM HEPES-NaOH pH 7.9, 5 mM EDTA, 1.2% SDS, 1 mM PMSF, 2 mM DTT, 1×Roche Complete

Protease Inhibitor Cocktail). The lysis solution was boiled for 20 minutes, followed by rapid chilling on ice. Centrifugation at 4,000*g* for 20 min at 4°C was performed twice and the final supernatant diluted 4-fold by adding 10 mM Tris-HCl pH 8.0, 150 mM NaCl, 1% Triton-X 100. 100 µg of c-Myc Antibody (9E10, sc-40, Santa Cruz) were added to the diluted extract (~160 ml) in 15 ml tubes and incubated for 8 hours at 4°C with rotation. 1.6 ml of 50% Protein G-Sepharose slurry (71-7083-00, GE Healthcare) was added and incubated overnight at 4°C with rotation. A mock control (no antibody) was performed to validate immunoprecipitation efficiency and specificity at small scale, using western blotting with mouse monoclonal c-Myc antibodies (9E10, sc-40, Santa Cruz) or c-Myc Antibody HRP conjugates (sc-40 HRP, Santa Cruz). Following immunoprecipitation, protein G beads were collected by centrifugation at 500*g* for 1 minute and washed five times with wash buffer (1% Triton X-100, 15 mM Tris-HCl, pH 8.0, 150 mM NaCl, 1 mM EDTA). Immunocomplexes were eluted from the Protein G beads by incubation at 70°C for 15 minutes in 2 volumes of elution buffer (100 mM Tris-Cl, 1 mM $CaCl_2$, 10 mM EDTA, 0.5 % SDS). 20 µg/ml of proteinase K was added to the beads and incubated at 50°C for 4 hours with occasional mixing. An equal volume of phenol/chloroform was added to beads, vortexed and centrifuged at 16,000*g* for 10 minutes. The supernatant was transferred to a fresh 1.5 ml tube and phenol/chloroform extraction was repeated. SPO11-1-oligonucleotides were precipitated using 0.1 volume of 3 M sodium acetate pH 5.2, 7.5 µg of glycoblue (Ambion AM9515) and an equal volume of isopropanol, followed by incubation at -80°C for 2 hours. SPO11-1-oligonucleotides were collected by centrifugation at 16,000*g* for 45 minutes at 4°C. After two 80% ethanol rinses the pellet was air-dried and resuspended in 30µl of distilled water. 40µl of 2×formamide loading buffer (80% deionized formamide, 10 mM EDTA, pH 8.0, 0.5 mg/ml xylene cyanol FF, 10% saturated bromophenol blue) were added, mixed and incubated at 70°C for 5 minutes. SPO11-1-oligonucleotides and a 20 bp ladder were separated using a 10% TBE-Urea gel (Invitrogen EC6875BOX) and stained by SYBR® Gold Nucleic Acid Gel Stain (Molecular Probes S-11494) for 3 minutes

682 with gentle shaking. The gel region corresponding to 35–50 nt was excised, macerated and
683 soaked in 10 mM Tris (pH 8.0) overnight at 37°C with rotation. The gel fragments were
684 removed by SpinX-centrifuge tube filters (Costar 8163) and the eluate was transferred to
685 fresh 1.5 ml tubes. 0.3 volume of 9 M ammonium acetate, 7.5 µg of glycoblue and 2.5
686 volumes of 100% ethanol were added, mixed and incubated at -80°C for 2 hours. The size-
687 selected SPO11-1-oligonucleotides were centrifuged at 16,000*g* for 45 minutes as above,
688 rinsed twice by 80% ethanol, air-dried and dissolved in 40 µl of distilled water.
689
690 For end-labelling experiments an aliquot (50 µl) of Protein G beads reserved from the
691 immunoprecipitation was washed twice with 1×terminal deoxynucleotidyl transferase (TdT)
692 buffer (50 mM potassium acetate, 20 mM Tris-acetate, 10 mM magnesium acetate, pH 7.9),
693 and incubated with 15 units of TdT (M0315L, NEB), 50 µCi [α-32P]-dCTP triphosphate
694 (5,000 Ci/mmol) and 5 µl of 10×TdT buffer, in a total volume of 50 µl, for 30 minutes at 37°C.
695 The beads were washed three times with wash buffer. SPO11-1-oligonucleotide complexes
696 were eluted by boiling for 3 minutes in 50 µl of 2×Laemmli buffer and separated using a 10%
697 SDS-PAGE gel. The gel was vacuum-dried and radioactivity was detected by exposing to a
698 phosphoimager screen.
699
700 **SPO11-1-oligonucleotide library construction**
701 Approximately 1 pmol of purified SPO11-1-oligonucleotides were used for GTP tailing at their
702 3′-ends. Conditions were used such that between 3 and 5 GMP residues were added per
703 oligonucleotide. A 40 µl reaction was used containing 1×TdT buffer (50 mM potassium
704 acetate, 20 mM Tris-acetate, 10 mM magnesium acetate, pH 7.9), 20 units of TdT (M0315L,
705 NEB), and 2 mM GTP at 37°C for 6 hours. TdT was inactivated by incubating at 75°C for 10
706 minutes. The G-tailed oligonucleotides were precipitated by incubating with 2.5 volumes of
707 100% ethanol and 0.3 volumes of 9 M ammonium acetate at -80°C for 2 hours, followed by

centrifugation at 16,000*g* for 45 minutes, washing twice with 80% ethanol, air-drying and resuspension in 20 µl of distilled water. G-tailed SPO11-1-oligonucleotides were ligated to a double-stranded DNA adapter in a 40 µl reaction of 1×T4 RNA ligase 2 buffer (50 mM Tris-HCl pH 7.5, 2 mM $MgCl_2$, 1 mM DTT, 400 µM ATP), 10 pmol double-stranded 3′ adapter (3'-adapter: top strand, 5′-pTGGAATTCTCGGGTGCCAAGGddC-3′, bottom strand, 5′-AGCCTTGGCACCCGAGAATTCCACCC-3′) (Supplementary Table 14) and 20 units of T4 RNA ligase 2 (dsRNA ligase) (M0239L, NEB) overnight at room temperature. To synthesize complementary strands of SPO11-1-oligonucleotides, 30 µM dNTP and 10 units of Klenow polymerase (NEB) were added to the ligation reaction, incubated at 25°C for 15 minutes, followed by 70°C for 10 minutes. 0.3 volumes of 9 M ammonium acetate, 5 µg of glycoblue and 2.5 volumes of 100% ethanol were added, and DNA precipitated at -80°C for 2 hours, followed by centrifugation at 16,000*g*. The pellet was washed twice with 80% ethanol, air-dried and re-dissolved in 20 µl of water. 30 µl of formamide loading buffer was added, mixed and incubated at 70°C for 5 minutes. The denatured products were separated by electrophoresis using a 10% TBE-Urea gel, and the gel region between 60–80 nt (equivalent to 32–52 nt SPO11-1-oligonucleotides with (rG)3-5 tails and a ligated 23 nucleotide adapter) was excised, macerated and rotated overnight at 37°C overnight in 400 µl of 10 mM Tris-HCl, pH 8.0. The buffer containing dissolved SPO11-1-oligonucleotides was centrifuged through SpinX-centrifuge tube filters. 0.3 volumes of 9 M ammonium acetate, 10 µg of glycoblue, and 2.5 volumes of 100% ethanol were added and DNA was precipitated at -80°C for 2 hours, followed by centrifugation at 16,000*g* for 45 minutes. The pellet was washed twice with 70% ethanol and air-dried. The 3′-ends of gel-purified denatured DNA strands were tailed with GTP by dissolving the dried pellet in a 40 µl tailing reaction containing 1×TnT buffer, 30 units of TdT, and 50 µM GTP, then incubating at 37°C for 6 hours and at 70°C for 10 minutes. The G-tailed products were precipitated with 0.3 volumes of 9 M ammonium acetate, 10 µg of glycoblue, and 2.5 volumes of 100% ethanol at -80°C for 2 hours, followed

by centrifugation at 16,000*g* for 45 minutes. After washing with 70% ethanol twice, the air-dried pellet was dissolved in 20 µl of distilled water and incubated in 40 µl of 1×T4 RNA ligase 2 buffer, 10 pmol double-stranded DNA adapter (5′ adapter: top strand, 5′-pATCGTCGGACTGTAGAACTCTGAAddC-3′. bottom strand, 5′-AGTTCAGAGTTCTACAGTCCGACGATCCC-3′) (Supplementary Table 14) and 30 units of T4 RNA ligase2 at room temperature overnight. Finally 30 µM dNTP and 10 units of Klenow polymerase were added and incubated at 25˚C for 15 minutes, followed by 70˚C for 10 minutes.

A test PCR was performed using a total reaction volume of 20 µl with 1/50 of the final Klenow reaction, 1×FailSafe™ PCR 2×PreMix E (FSP995E, Epicentre), 1µl of Pfu Ultra II Fusion HS DNA Polymerase (Catalog #600672, Agilent) and 1 µM primers RP1 and RPI1. The reaction mixture was divided into two tubes, and PCR performed at 94°C for 20 seconds, followed by 20 cycles of {94°C for 10 seconds; 60°C for 30 seconds; 72°C for 15 seconds}. 5 µl of the PCR products were separated using a 10% TBE gel (EC6275BOX, Invitrogen) with a PCR 20 bp low ladder (P1598, Sigma-Aldrich) and stained with SYBR gold to determine the size and quantity of PCR products. PCRs were then scaled up to a total volume of 400 µl. This mixture was divided into 10 µl aliquots, denatured at 94°C for 10 seconds and amplified for 16 cycles of {94°C for 10 seconds; 60°C for 30 seconds; 72°C for 15 seconds}. PCR products were pooled and precipitated using 0.3 volumes of 9 M ammonium acetate, 7.5 µg of glycoblue and 2.5 volumes of 100% ethanol. The PCR products were separated by electrophoresis using a 10% TBE gel, and the gel area corresponding to 160–180 bp was excised, macerated and soaked in 400 µl of 10 mM Tris, pH 8.0 at 37˚C overnight, with mixing. The eluate was spun through a SpinX-centrifuge tube filter and DNA was precipitated using 0.3 volume of 9 M ammonium acetate, 7.5 µg of glycoblue and 2.5 volumes of 100%

ethanol. The air-dried DNA pellet was dissolved in 30 µl of 10 mM Tris, pH 8.0. Sequencing was performed using an Illumina NextSeq instrument.

MNase and H3K4^{me3} chromatin immunoprecipitation sequencing

Micrococcal nuclease digestion and sequencing library construction were performed as reported(Choi et al. 2016). For ChIP two grams of unopened floral buds were ground in liquid nitrogen. Nuclei were isolated and *in vitro* cross-linked in nuclear isolation crosslinking buffer (60 mM Hepes pH 8.0, 1 M sucrose, 5 mM KCl, 5 mM $MgCl_2$, 5 mM EDTA, 0.6% Triton X-100, 0.4 mM PMSF, 1 ug pepstatin, 1×protein inhibitor cocktails, 1% formaldehyde) at room temperature for 25 minutes. Glycine was added to a final concentration of 125 mM and incubated for 25 minutes at room temperature with rotation. Cross-linked bud lysate was filtered through one layer of Miracloth and centrifuged at 2,000*g* at 4°C for 20 minutes. The pellet was resuspended in extraction buffer (0.25 M sucrose, 10 mM Tris-HCl pH 8.0, 10 mM $MgCl_2$, 1% Triton X-100, 1 mM EDTA, 5 mM β-mercaptoethanol, 0.1 mM PMSF, 1×proteinase inhibitor cocktails) and centrifuged at 2,000*g* at 4°C for 15 minutes. The nuclei pellet was rinsed with 1 ml of TNE buffer (10 mM Tris-HCl pH 8.0, 10 mM NaCl, 1 mM EDTA, 1×proteinase inhibitor cocktails), resuspended and then centrifuging at 2,000*g* at 4°C for 5 minutes. Cross-linked chromatin was digested with 0.05 units of mirococcal nuclease (MNase, NEB M0247S) in reaction buffer (10 mM Tris-HCl, pH 8.0, 10 mM NaCl, 1 mM EDTA, 4 mM $CaCl_2$) at 37°C for 15 minutes with vortexing. The reaction was stopped by adding EDTA to a final concentration of 20 mM, vortexing and placing on ice for 10 minutes. One volume of 10 mM Tris-pH 8, 0.2% SDS, 2% Triton X-100, 0.2% sodium deoxycholate, 1×proteinase inhibitor cocktails was added and rotated for 2 hours at 4°C. The reactions were centrifuged at 14,000*g* in a microfuge for 5 minutes at 4°C. The supernatant was used for immunoprecipitation overnight at 4°C using Dynabeads Protein G that were pre-bound to 5 µg H3K4^{me3} antibody (AbCam ab8580). The chromatin immunocomplexes were washed,

eluted and reverse-crosslinked. The immunoprecipitates were further purified by phenol/chlorophorm/isoamyl alcohol (24:24:1) extraction, followed by ethanol precipitation and 2% agarose gel separation and gel extraction of ~145–150 bp DNA. Approximately 10 ng of ChIP-purified DNA was used to generate a library using the TruSeq Prep Kit v2 (Illumina). Libraries were subjected to paired-end sequenced using an Illumina NextSeq instrument.

RNA-sequencing

Five µg of total RNA from unopened flower buds were extracted using Trizol reagent. To perform rRNA depletion we used the Ribo-Zero magnetic kit (MRZPL116). Fifty ng of rRNA-depleted RNA were used for RNA-seq library construction using the ScriptSeq v2 RNA-seq Library Preparation Kit (SSV21124). The library was amplified using 12 PCR cycles and indexed using ScriptSeq Index PCR Primers (RSBC10948) and FailSafeTM PCR Enzyme Mix (FSE51100). Sequencing was performed on a HiSeq instrument. RNA-seq data were analyzed using RSem.

Bioinformatics analysis of SPO11-1-oligonucleotides, ChIP-seq and MNase-seq data

For SPO11-1-oligonucleotide data FASTQ files were trimmed for 3′-adapter sequences using the FASTX-Toolkit function fastx_clipper (http://hannonlab.cshl.edu/fastx_toolkit/). For the wild type libraries RPI1 and RPI3 5 bp were trimmed from the read 5′-ends, while for other libraries 10 bp were cropped, due to longer adapter sequences. Trimmed reads were aligned to the TAIR10 reference sequence using bowtie2 with the following settings: --very-sensitive -p 4 -k 10. Aligned reads were filtered to have 2 or fewer mismatches. Reads with the SAM optional field “XS:i” were dropped to obtain unique alignments. Reads with multiple valid alignments were filtered for MAPQ scores of 10 or higher, and the highest value alignment kept. In the event that a read had multiple alignments with equal MAPQ scores, one was

randomly chosen. Unique and multiply aligning reads were then deduplicated using SAMtools. BAM files for uniquely and multiply aligning reads were combined. For MNase-seq and ChIP-seq data paired-end FASTQ files were directly aligned to the TAIR10 reference sequence using bowtie2 with the following settings --very-sensitive --no-discordant --no-mixed -p 4 -k 10. To obtain uniquely aligning reads, reads with the SAM optional field "XS:i" and MAPQ scores of less than 42 were dropped. To ensure reads were kept in proper pairs, a Python script was applied. Reads with multiple valid alignments were filtered for those with MAPQ scores of 10 or higher and the highest value alignments kept. Multiply aligning reads were treated as for SPO11-1-oligonucleotides. Unique and multiply aligning reads were then deduplicated using SAMtools, combined and used for downstream analysis. Coverage values from these reads were calculated using Rsamtools and normalized by the sum of coverage per library. Analysis of these data in relation to features including TAIR10 representative gene TSS and TTS and transposons(Buisine et al. 2008), was performed as previously described (Choi et al. 2013). For hexile analysis normalized values of SPO11-1-oligonucleotides were calculated in windows -500 bp upstream of TSS for promoters or +500 bp downstream of TTS for terminators. These regions were also measured for nucleosome occupancy and AT-rich motif matches. These were compared with H3K4^{me3} and CTT motif matches in the 500 bp downstream of TSS and upstream of TTS. To test the extent of SPO11-1-oligonucleotide hexile overlap with crossovers, we used a set of 2,499 crossovers mapped using genotyping-by-sequencing in Col×Ler F_2 individuals(Choi et al. 2016; Yelina et al. 2015). SPO11-1 levels were calculated within each SNP interval used to detect crossovers. Intervals were also classified according to their overlap with genomic annotation and position along chromosomes in 2 megabase bands. Data were modeled with the glm function in R, using the binomial family and a logistic link function.

837 **Data Access**

838 The FASTQ files associated with the genomic datasets described here have been uploaded
839 to the ArrayExpress repositories, and can be accessed using the provided usernames and
840 passwords.

841 SPO11-1-oligonucleotides: https://www.ebi.ac.uk/arrayexpress/experiments/E-MTAB-5041/

842 Username: Reviewer_E-MTAB-5041 Password: MKE8bvew

843 Nucleosome MNase-seq: https://www.ebi.ac.uk/arrayexpress/experiments/E-MTAB-5042/

844 Username: Reviewer_E-MTAB-5042 Password: 4c0zvhju

845 H3K4^{me3} ChIP-seq: https://www.ebi.ac.uk/arrayexpress/experiments/E-MTAB-5048/

846 Username: Reviewer_E-MTAB-5048 Password: 4c0zvhju

847 RNA-seq: https://www.ebi.ac.uk/arrayexpress/experiments/E-MTAB-5417/

848 Username: Reviewer_E-MTAB-5417 Password: 2rX8I48v

849

850 **Acknowledgements**

851 Research was supported by a Royal Society University Research Fellowship, the Gatsby
852 Charitable Foundation grant GAT2962, BBSRC grant BB/N007557/1, National Natural
853 Science Foundation of China grant 61403318, Next-Generation BioGreen Program (SSAC
854 grant PJ01137901 RDA Korea) and an EMBO long-term postdoctoral fellowship (ALT 807-
855 2009).

856

857 **Author Contributions**

858 KC, CL, CJU, HS, PAZ, NEY, RAM and IRH contributed to design of the study. KC, CL, CJU
859 and HS performed experiments. KC, XZ, CL, CJU, TJH, HS, AJT, RAM and IRH analyzed
860 the data. KC, XZ, CL CJU, TJH, HS, AJT, PAZ, NEY, RAM and IRH wrote the manuscript.

861

862

References

Acquaviva L, Székvölgyi L, Dichtl B, Dichtl BS, de La Roche Saint André C, Nicolas A, Géli V. 2013. The COMPASS subunit Spp1 links histone methylation to initiation of meiotic recombination. *Science* **339**: 215–8.

Alonso-Blanco C, Andrade J, Becker C, Bemm F, Bergelson J, Borgwardt KMM, Cao J, Chae E, Dezwaan TMM, Ding W, et al. 2016. 1,135 Genomes Reveal the Global Pattern of Polymorphism in Arabidopsis thaliana. *Cell* **166**: 481–491.

Armstrong SJ, Caryl AP, Jones GH, Franklin FCH. 2002. Asy1, a protein required for meiotic chromosome synapsis, localizes to axis-associated chromatin in Arabidopsis and Brassica. *J Cell Sci* **115**: 3645–55.

Baker CL, Walker M, Kajita S, Petkov PM, Paigen K. 2014. PRDM9 binding organizes hotspot nucleosomes and limits Holliday junction migration. *Genome Res* **24**: 724–732.

Barton NH, Charlesworth B. 1998. Why sex and recombination? *Science* **281**: 1986–90.

Baudat F, Buard J, Grey C, Fledel-Alon A, Ober C, Przeworski M, Coop G, de Massy B. 2010. PRDM9 is a major determinant of meiotic recombination hotspots in humans and mice. *Science* **327**: 836–40.

Baudat F, Imai Y, de Massy B. 2013. Meiotic recombination in mammals: localization and regulation. *Nat Rev Genet* **14**: 794–806.

Beauregard A, Curcio MJ, Belfort M. 2008. The Take and Give Between Retrotransposable Elements and their Hosts. *Annu Rev Genet* **42**: 587–617.

Berchowitz LE, Copenhaver GP. 2008. Fluorescent Arabidopsis tetrads: a visual assay for quickly developing large crossover and crossover interference data sets. *Nat Protoc* **3**: 41–50.

Bloom KS. 2014. Centromeric Heterochromatin: The Primordial Segregation Machine. *Annu Rev Genet* **48**: 457–484.

Borde V, Robine N, Lin W, Bonfils S, Géli V, Nicolas A. 2009. Histone H3 lysine 4 trimethylation marks meiotic recombination initiation sites. *EMBO J* **28**: 99–111.

Borhan MH, Gunn N, Cooper A, Gulden S, Tör M, Rimmer SR, Holub EB. 2008. WRR4 encodes a TIR-NB-LRR protein that confers broad-spectrum white rust resistance in Arabidopsis thaliana to four physiological races of Albugo candida. *Mol Plant Microbe Interact* **21**: 757–68.

Brick K, Smagulova F, Khil P, Camerini-Otero RD, Petukhova G V. 2012. Genetic recombination is directed away from functional genomic elements in mice. *Nature* **485**: 642–5.

Buisine N, Quesneville H, Colot V. 2008. Improved detection and annotation of transposable elements in sequenced genomes using multiple reference sequence sets. *Genomics* **91**: 467–75.

Cheng C-Y, Krishnakumar V, Chan AP, Thibaud-Nissen F, Schobel S, Town CD. 2017. Araport11: a complete reannotation of the *Arabidopsis thaliana* reference genome. *Plant J* **89**: 789–804.

Choi K, Henderson IR. 2015. Meiotic recombination hotspots - a comparative view. *Plant J* **83**: 52–61.

Choi K, Reinhard C, Serra H, Ziolkowski PA, Underwood CJ, Zhao X, Hardcastle TJ, Yelina NE, Griffin C, Jackson M, et al. 2016. Recombination Rate Heterogeneity within Arabidopsis Disease Resistance Genes. *PLOS Genet* **12**: e1006179.

Choi K, Zhao X, Kelly KA, Venn O, Higgins JD, Yelina NE, Hardcastle TJ, Ziolkowski PA, Copenhaver GP, Franklin FCH, et al. 2013. Arabidopsis meiotic crossover hot spots overlap with H2A.Z nucleosomes at gene promoters. *Nat Genet* **45**: 1327–36.

Choulet F, Alberti A, Theil S, Glover N, Barbe V, Daron J, Pingault L, Sourdille P, Couloux A, Paux E, et al. 2014. Structural and functional partitioning of bread wheat chromosome 3B. *Science* **345**: 1249721.

Cooper TJ, Garcia V, Neale MJ. 2016. Meiotic DSB patterning: A multifaceted process. *Cell Cycle* **15**: 13–21.

Copenhaver GP, Nickel K, Kuromori T, Benito MI, Kaul S, Lin X, Bevan M, Murphy G, Harris B, Parnell LD, et al. 1999. Genetic definition and sequence analysis of Arabidopsis centromeres. *Science* **286**: 2468–74.

De Massy B. 2013. Initiation of meiotic recombination: how and where? Conservation and specificities among eukaryotes. *Annu Rev Genet* **47**: 563–99.

Drouaud J, Khademian H, Giraut L, Zanni V, Bellalou S, Henderson IR, Falque M, Mézard C. 2013. Contrasted patterns of crossover and non-crossover at Arabidopsis thaliana meiotic recombination hotspots. *PLoS Genet* **9**: e1003922.

Fan QQ, Petes TD. 1996. Relationship between nuclease-hypersensitive sites and meiotic recombination hot spot activity at the HIS4 locus of Saccharomyces cerevisiae. *Mol Cell Biol* **16**: 2037–43.

Feschotte C, Mouchès C. 2000. Evidence that a family of miniature inverted-repeat transposable elements (MITEs) from the Arabidopsis thaliana genome has arisen from a pogo-like DNA transposon. *Mol Biol Evol* **17**: 730–7.

Feschotte C, Pritham EJ. 2007. DNA Transposons and the Evolution of Eukaryotic Genomes. *Annu Rev Genet* **41**: 331–368.

Fowler KR, Sasaki M, Milman N, Keeney S, Smith GR. 2014. Evolutionarily diverse determinants of meiotic DNA break and recombination landscapes across the genome. *Genome Res* **24**: 1650–64.

Fu H, Zheng Z, Dooner HK. 2002. Recombination rates between adjacent genic and retrotransposon regions in maize vary by 2 orders of magnitude. *Proc Natl Acad Sci U S A* **99**: 1082–1087.

Garcia V, Phelps SEL, Gray S, Neale MJ. 2011. Bidirectional resection of DNA double-strand breaks by Mre11 and Exo1. *Nature* **479**: 241–4.

Giraut L, Falque M, Drouaud J, Pereira L, Martin OC, Mézard C. 2011. Genome-wide crossover distribution in Arabidopsis thaliana meiosis reveals sex-specific patterns along chromosomes. *PLoS Genet* **7**: e1002354.

Grelon M, Vezon D, Gendrot G, Pelletier G. 2001. AtSPO11-1 is necessary for efficient meiotic recombination in plants. *EMBO J* **20**: 589–600.

Grey C, Barthès P, Chauveau-Le Friec G, Langa F, Baudat F, de Massy B. 2011. Mouse PRDM9 DNA-binding specificity determines sites of histone H3 lysine 4 trimethylation for initiation of meiotic recombination. *PLoS Biol* **9**: e1001176.

Grey C, Clément JAJ, Buard J, Leblanc B, Gut I, Gut M, Duret L, de Massy B. 2017. In vivo binding of PRDM9 reveals interactions with noncanonical genomic sites. *Genome Res* **27**: 580–590.

Guermonprez H, Loot C, Casacuberta JM. 2008. Different strategies to persist: the pogo-like Lemi1 transposon produces miniature inverted-repeat transposable elements or typical defective elements in different plant genomes. *Genetics* **180**: 83–92.

Hamilton W. 2002. *Narrow Roads Of Gene Land, Volume 2: Evolution Of Sex*. Oxford University Press, Oxford.

Hartung F, Wurz-Wildersinn R, Fuchs J, Schubert I, Suer S, Puchta H. 2007. The catalytically active tyrosine residues of both SPO11-1 and SPO11-2 are required for meiotic double-strand break induction in Arabidopsis. *Plant Cell* **19**: 3090–9.

Hellsten U, Wright KM, Jenkins J, Shu S, Yuan Y, Wessler SR, Schmutz J, Willis JH, Rokhsar DS. 2013. Fine-scale variation in meiotic recombination in Mimulus inferred from population shotgun sequencing. *Proc Natl Acad Sci U S A* **110**: 19478–82.

Horton MW, Hancock AM, Huang YS, Toomajian C, Atwell S, Auton A, Muliyati NW, Platt A, Sperone FG, Vilhjálmsson BJ, et al. 2012. Genome-wide patterns of genetic variation in worldwide Arabidopsis thaliana accessions from the RegMap panel. *Nat Genet* **44**: 212–6.

Imai Y, Baudat F, Taillepierre M, Stanzione M, Toth A, de Massy B. 2017. The PRDM9 KRAB domain is required for meiosis and involved in protein interactions. *Chromosoma*.

968 Jones JDG, Dangl JL. 2006. The plant immune system. *Nature* **444**: 323–329.

969 Kankel MW, Ramsey DE, Stokes TL, Flowers SK, Haag JR, Jeddeloh JA, Riddle NC,
970 Verbsky ML, Richards EJ. 2003. Arabidopsis MET1 cytosine methyltransferase
971 mutants. *Genetics* **163**: 1109–1122.

972 Kapitonov V V, Jurka J. 2001. Rolling-circle transposons in eukaryotes. *Proc Natl Acad Sci U*
973 *S A* **98**: 8714–9.

974 Kato M, Miura A, Bender J, Jacobsen SE, Kakutani T. 2003. Role of CG and non-CG
975 methylation in immobilization of transposons in Arabidopsis. *Curr Biol* **13**: 421–6.

976 Kauppi L, Jeffreys AJ, Keeney S. 2004. Where the crossovers are: recombination
977 distributions in mammals. *Nat Rev Genet* **5**: 413–24.

978 Kawakatsu T, Huang S-SC, Jupe F, Sasaki E, Schmitz RJ, Urich MA, Castanon R, Nery JR,
979 Barragan C, He Y, et al. 2016. Epigenomic Diversity in a Global Collection of
980 Arabidopsis thaliana Accessions. *Cell* **166**: 492–505.

981 Keeney S, Giroux CN, Kleckner N. 1997. Meiosis-specific DNA double-strand breaks are
982 catalyzed by Spo11, a member of a widely conserved protein family. *Cell* **88**: 375–84.

983 Keeney S, Kleckner N. 1995. Covalent protein-DNA complexes at the 5' strand termini of
984 meiosis-specific double-strand breaks in yeast. *Proc Natl Acad Sci U S A* **92**: 11274–8.

985 Kong A, Thorleifsson G, Gudbjartsson DF, Masson G, Sigurdsson A, Jonasdottir A, Walters
986 GB, Jonasdottir A, Gylfason A, Kristinsson KT, et al. 2010. Fine-scale recombination
987 rate differences between sexes, populations and individuals. *Nature* **467**: 1099–103.

988 Lam I, Keeney S. 2014. Mechanism and Regulation of Meiotic Recombination Initiation. *Cold*
989 *Spring Harb Perspect Biol* **7**: a016634.

990 Lam I, Keeney S. 2015. Nonparadoxical evolutionary stability of the recombination initiation
991 landscape in yeast. *Science* **350**: 932–7.

992 Lange J, Yamada S, Tischfield SE, Pan J, Kim S, Zhu X, Socci ND, Jasin M, Keeney S.
993 2016. The Landscape of Mouse Meiotic Double-Strand Break Formation, Processing,
994 and Repair. *Cell* **167**: 695–708.e16.

995 Liu S, Yeh C-T, Ji T, Ying K, Wu H, Tang HM, Fu Y, Nettleton D, Schnable PS. 2009. Mu
996 Transposon Insertion Sites and Meiotic Recombination Events Co-Localize with
997 Epigenetic Marks for Open Chromatin across the Maize Genome. *PLoS Genet* **5**: 13.

998 Malik HS, Henikoff S. 2009. Major Evolutionary Transitions in Centromere Complexity. *Cell*
999 **138**: 1067–1082.

1000 Mathieu O, Reinders J, Caikovski M, Smathajitt C, Paszkowski J. 2007. Transgenerational
1001 stability of the Arabidopsis epigenome is coordinated by CG methylation. *Cell* **130**: 851–
1002 62.

1003 McClintock B. 1956. Controlling Elements and the Gene. *Cold Spring Harb Symp Quant Biol*
1004 **21**: 197–216.

1005 Mihola O, Trachtulec Z, Vlcek C, Schimenti JC, Forejt J. 2009. A mouse speciation gene
1006 encodes a meiotic histone H3 methyltransferase. *Science* **323**: 373–5.

1007 Myers S, Bottolo L, Freeman C, McVean G, Donnelly P. 2005. A fine-scale map of
1008 recombination rates and hotspots across the human genome. *Science* **310**: 321–4.

1009 Myers S, Bowden R, Tumian A, Bontrop RE, Freeman C, MacFie TS, McVean G, Donnelly
1010 P. 2010. Drive against hotspot motifs in primates implicates the PRDM9 gene in meiotic
1011 recombination. *Science* **327**: 876–9.

1012 Myers S, Freeman C, Auton A, Donnelly P, McVean G. 2008. A common sequence motif
1013 associated with recombination hot spots and genome instability in humans. *Nat Genet*
1014 **40**: 1124–9.

1015 Neale MJ, Keeney S. 2009. End-labeling and analysis of Spo11-oligonucleotide complexes
1016 in Saccharomyces cerevisiae. *Methods Mol Biol* **557**: 183–95.

1017 Neale MJ, Pan J, Keeney S. 2005. Endonucleolytic processing of covalent protein-linked
1018 DNA double-strand breaks. *Nature* **436**: 1053–7.

1019 Nicolas A, Treco D, Schultes NP, Szostak JW. 1989. An initiation site for meiotic gene
1020 conversion in the yeast Saccharomyces cerevisiae. *Nature* **338**: 35–9.

1021 Pan J, Sasaki M, Kniewel R, Murakami H, Blitzblau HG, Tischfield SE, Zhu X, Neale MJ,
1022 Jasin M, Socci ND, et al. 2011. A hierarchical combination of factors shapes the
1023 genome-wide topography of yeast meiotic recombination initiation. *Cell* **144**: 719–31.

1024 Parvanov ED, Petkov PM, Paigen K. 2010. Prdm9 controls activation of mammalian
1025 recombination hotspots. *Science* **327**: 835.

1026 Powers NR, Parvanov ED, Baker CL, Walker M, Petkov PM, Paigen K. 2016. The Meiotic
1027 Recombination Activator PRDM9 Trimethylates Both H3K36 and H3K4 at
1028 Recombination Hotspots In Vivo ed. I.R. Adams. *PLOS Genet* **12**: e1006146.

1029 Quadrana L, Bortolini Silveira A, Mayhew GF, LeBlanc C, Martienssen RA, Jeddeloh JA,
1030 Colot V. 2016. The Arabidopsis thaliana mobilome and its impact at the species level.
1031 *Elife* **5**.

1032 Robert T, Nore A, Brun C, Maffre C, Crimi B, Bourbon H-M, de Massy B. 2016. The
1033 TopoVIB-Like protein family is required for meiotic DNA double-strand break formation.
1034 *Science (80-)* **351**: 943–949.

1035 Rowan BA, Patel V, Weigel D, Schneeberger K. 2015. Rapid and Inexpensive Whole-
1036 Genome Genotyping-by-Sequencing for Crossover Localization and Fine-Scale Genetic
1037 Mapping. *G3 (Bethesda)* **5**: 385–98.

1038 Salomé PA, Bomblies K, Fitz J, Laitinen RAE, Warthmann N, Yant L, Weigel D. 2012. The
1039 recombination landscape in Arabidopsis thaliana F2 populations. *Heredity (Edinb)* **108**:
1040 447–55.

1041 Sanchez-Moran E, Santos J-L, Jones GH, Franklin FCH. 2007. ASY1 mediates AtDMC1-
1042 dependent interhomolog recombination during meiosis in Arabidopsis. *Genes Dev* **21**:
1043 2220–33.

1044 Sasaki M, Lange J, Keeney S. 2010. Genome destabilization by homologous recombination
1045 in the germline. *Nat Rev Mol Cell Biol* **11**: 182.

1046 Sasaki M, Tischfield SE, van Overbeek M, Keeney S. 2013. Meiotic recombination initiation
1047 in and around retrotransposable elements in Saccharomyces cerevisiae. *PLoS Genet* **9**:
1048 e1003732.

1049 Saze H, Mittelsten Scheid O, Paszkowski J. 2003. Maintenance of CpG methylation is
1050 essential for epigenetic inheritance during plant gametogenesis. *Nat Genet* **34**: 65–9.

1051 Segal E, Widom J. 2009. Poly(dA:dT) tracts: major determinants of nucleosome organization.
1052 *Curr Opin Struct Biol* **19**: 65–71.

1053 Shi J, Wolf SE, Burke JM, Presting GG, Ross-Ibarra J, Dawe RK. 2010. Widespread gene
1054 conversion in centromere cores. *PLoS Biol* **8**: e1000327.

1055 Shilo S, Melamed-Bessudo C, Dorone Y, Barkai N, Levy AA. 2015. DNA Crossover Motifs
1056 Associated with Epigenetic Modifications Delineate Open Chromatin Regions in
1057 Arabidopsis. *Plant Cell* **27**: tpc.15.00391.

1058 Silverstein KAT, Graham MA, Paape TD, VandenBosch KA. 2005. Genome organization of
1059 more than 300 defensin-like genes in Arabidopsis. *Plant Physiol* **138**: 600–10.

1060 Singhal S, Leffler EM, Sannareddy K, Turner I, Venn O, Hooper DM, Strand AI, Li Q, Raney
1061 B, Balakrishnan CN, et al. 2015. Stable recombination hotspots in birds. *Science (80-)*
1062 **350**: 928–932.

1063 Slotkin RK, Martienssen R. 2007. Transposable elements and the epigenetic regulation of
1064 the genome. *Nat Rev Genet* **8**: 272–85.

1065 Sommermeyer V, Béneut C, Chaplais E, Serrentino ME, Borde V. 2013. Spp1, a member of
1066 the Set1 Complex, promotes meiotic DSB formation in promoters by tethering histone
1067 H3K4 methylation sites to chromosome axes. *Mol Cell* **49**: 43–54.

1068 Stroud H, Greenberg MVC, Feng S, Bernatavichute Y V, Jacobsen SE. 2013.
1069 Comprehensive analysis of silencing mutants reveals complex regulation of the
1070 Arabidopsis methylome. *Cell* **152**: 352–64.

1071 Stuart T, Eichten S, Cahn J, Karpievitch Y, Borevitz J, Lister R. 2016. Population scale
1072 mapping of transposable element diversity reveals links to gene regulation and
1073 epigenomic variation. *Elife* **5**.

1074 Székvölgyi L, Ohta K, Nicolas A. 2015. Initiation of Meiotic Homologous Recombination:
1075 Flexibility, Impact of Histone Modifications, and Chromatin Remodeling. *Cold Spring*
1076 *Harb Perspect Biol* **7**: a016527.

1077 Szostak JW, Orr-Weaver TL, Rothstein RJ, Stahl FW. 1983. The double-strand-break repair
1078 model for recombination. *Cell* **33**: 25–35.

1079 Tischfield SE, Keeney S. 2012. Scale matters: the spatial correlation of yeast meiotic DNA
1080 breaks with histone H3 trimethylation is driven largely by independent colocalization at
1081 promoters. *Cell Cycle* **11**: 1496–503.

1082 Van der Biezen EA, Freddie CT, Kahn K, Parker JE, Jones JDG. 2002. Arabidopsis RPP4 is
1083 a member of the RPP5 multigene family of TIR-NB-LRR genes and confers downy
1084 mildew resistance through multiple signalling components. *Plant J* **29**: 439–51.

1085 Villeneuve AM, Hillers KJ. 2001. Whence meiosis? *Cell* **106**: 647–50.

1086 Vincenten N, Kuhl L-M, Lam I, Oke A, Kerr AR, Hochwagen A, Fung J, Keeney S, Vader G,
1087 Marston AL. 2015. The kinetochore prevents centromere-proximal crossover
1088 recombination during meiosis. *Elife* **4**.

1089 Vrielynck N, Chambon A, Vezon D, Pereira L, Chelysheva L, De Muyt A, Mézard C, Mayer
1090 C, Grelon M. 2016. A DNA topoisomerase VI-like complex initiates meiotic
1091 recombination. *Science* **351**: 939–43.

1092 Wijnker E, Velikkakam James G, Ding J, Becker F, Klasen JR, Rawat V, Rowan BA, de Jong
1093 DF, de Snoo CB, Zapata L, et al. 2013. The genomic landscape of meiotic crossovers
1094 and gene conversions in Arabidopsis thaliana. *Elife* **2**: e01426.

1095 Wu TC, Lichten M. 1994. Meiosis-induced double-strand break sites determined by yeast
1096 chromatin structure. *Science* **263**: 515–8.

1097 Yandeau-Nelson MD, Zhou Q, Yao H, Xu X, Nikolau BJ, Schnable PS. 2005. MuDR
1098 transposase increases the frequency of meiotic crossovers in the vicinity of a Mu
1099 insertion in the maize a1 gene. *Genetics* **169**: 917–29.

1100 Yelina NE, Lambing C, Hardcastle TJ, Zhao X, Santos B, Henderson IR. 2015. DNA
1101 methylation epigenetically silences crossover hot spots and controls chromosomal
1102 domains of meiotic recombination in Arabidopsis. *Genes Dev* **29**: 2183–202.

1103 Yelina NE, Ziolkowski PA, Miller N, Zhao X, Kelly KA, Muñoz DF, Mann DJ, Copenhaver GP,
1104 Henderson IR. 2013. High-throughput analysis of meiotic crossover frequency and
1105 interference via flow cytometry of fluorescent pollen in Arabidopsis thaliana. *Nat Protoc*
1106 **8**: 2119–2134.

1107 Zamudio N, Barau J, Teissandier A, Walter M, Borsos M, Servant N, Bourc'his D. 2015. DNA
1108 methylation restrains transposons from adopting a chromatin signature permissive for
1109 meiotic recombination. *Genes Dev* **29**: 1256–70.

Zhang X, Bernatavichute Y V, Cokus S, Pellegrini M, Jacobsen SE. 2009. Genome-wide analysis of mono-, di- and trimethylation of histone H3 lysine 4 in Arabidopsis thaliana. *Genome Biol* **10**: R62.

Ziolkowski PA, Berchowitz LE, Lambing C, Yelina NE, Zhao X, Kelly KA, Choi K, Ziolkowska L, June V, Sanchez-Moran E, et al. 2015. Juxtaposition of heterozygosity and homozygosity during meiosis causes reciprocal crossover remodeling via interference. *Elife* **4**: e03708.

Supplemental Material

Supplemental Figures S1–S6

Supplemental Tables S1–S14